https://doi.org/10.15407/ufm.22.01.003

L.B. ZUEV*, S.A. BARANNIKOVA,
V.I. DANILOV, and V.V. GORBATENKO**

Institute of Strength Physics and Materials Science, SB of the RAS,
2/4, Akademicheskiy Ave., 634055 Tomsk, Russian Federation

*lbz@ispms.tsc.ru, ** bsa@ispms.ru

PLASTICITY: FROM CRYSTAL LATTICE TO MACROSCOPIC PHENOMENA

New representations concerning plasticity physics in crystals are discussed. The model of plastic flow is suggested, which can describe its main regularities. With the use of the experimental investigation, it is shown that the plastic flow localization plays the role in the evolution of plastic deformation. Obtained data are explained with the application of the principles of nonequilibrium-systems' theory. The quasi-particle is introduced for the description of plasticity phenomenon. It is established the relation between plasticity characteristics of metals and their position in Periodic table of the elements. A new model is elaborated to address localized plastic-flow evolution in solids. The basic assumption of the proposed model is that the elementary plasticity acts evolving in the deforming of medium would generate acoustic emission pulses, which interact with the plasticity carriers and initiate new elementary shears. As found experimentally, the macrolocalization of plastic flow involves a variety of autowave processes. To address the phenomenon of localized plastic-flow autowaves, a new quasi-particle called 'autolocalizon' is introduced; the criterion of validity of the concept is assessed.

Keywords: alloys, deformation, creep, self-organization, strength, plasticity, localization, failure.

1. Introduction: Problems of Plasticity

The simplest analysis of numerous works devoted to elucidation of the nature of plastic deformation immediately shows that we are dealings with a very complex problem. There have been ample proofs of this view, but it is enough to recall only one of them. Everybody knows that the principles of quantum mechanics had been developed within twenty

Citation: L.B. Zuev, S.A. Barannikova, V.I. Danilov, and V.V. Gorbatenko, Plasticity: from Crystal Lattice to Macroscopic Phenomena, *Progress in Physics of Metals*, **22**, No. 1: 3–57 (2021)

years after their first mentioning by Planck in 1900 [1]. However, investigations of various aspects of plasticity phenomenon used in technology for about five millennia and studied carefully for no less than two centuries have not resulted in the development of a consistent plasticity theory.

The complexity of this problem is primarily due to its multilateral character [2, 3]. It is difficult to take into account that the plastically deforming medium changes its structure and mechanical properties during the deformation process. These changes encompass space scales from crystal lattice to macroscopic volume. The phase composition of an alloy may also change during plastic flow.

This problem is of interest for solid-state physics in general because plastic flow is a complex response of the deforming medium on external mechanical stresses. For understanding and correct description of this response, fundamental principles of mechanics, crystallography, thermodynamics, quantum mechanics, hydrodynamics, materials science, and other scientific branches have to be used.

Why does plasticity physics remain enigmatic at present, almost 200-year-old history of scientific research? The key problem is to reconcile two opposite traditional approaches to plasticity. First of this is the approach of mechanics. It is characterized by a variety of employed macroscale models (*e.g.*, see [2, 3]), often very simplified. Characteristic scale of studying objects is of about 0.1–1 m in this case. The models quite often have only a pragmatic substantiation and are focused on solving particular problems of plastic deformation. Within the framework of these approaches, narrow practical aims can be achieved, obviously insufficient for understanding of the nature of plasticity.

Physical approaches to the plasticity [4–6] are mostly based on electron microscopic studies of small volumes in a deformed crystal [7]. In this case, typical scale of objects is about 10^{-6} m. Microstructural data obtained in these experiments are extrapolated without doubt, as usual, to a macroscopic volume. Similar procedure is not always well substantiated, and no agreement of scales has been achieved. Nevertheless, it is importantly that the microscopic aspect of the problem has been studied much better than macroscopic one [4–10].

Even taken together, these approaches have not yet led to a complete understanding of the problem. Amazing difference in scales hinders the progress. Results obtained to date only set limits for the mechanical and physical approaches. This situation is a challenge to a large number of researchers. This suggests that today physics of plasticity is open to new ideas and approaches. Recent approaches to a solution of the plasticity problem are aimed to reconcile the micro- and macroscopic models of a description of plastic flow. The new point of view on the plasticity is that microscopic interactions of defects described suffi-

ciently exactly can spontaneously generate some macroscopic features (structures). The principal ideas of this approach and their experimental confirmations are discussed in this work.

2. Plastic Flow Localization: Qualitative Analysis

The remarkable advance in the plasticity physics began when it was realised that this phenomenon is the part of a general problem devoted to the behaviour of a matter in the condition far from the equilibrium. Similar view does its interesting for other fields of science, since plastic flow is a response of an open nonequilibrium medium on external impact that can be studied comparatively easily.

2.1. Plastic Deformation and Synergetics

The decisive step was undertaken in 1987 when Seeger and Frank [11] have proposed to consider plastic flow as a process of structurization. They have declared as follow, '*The use of thermodynamics of irreversible processes in open systems to a description of structurization during plastic deformation of crystal materials is quite promising on qualitative level*'. This statement opened the way to using of synergetic methods in plasticity physics [12–15]. The attractiveness of this idea has been explained by the well-known progress in understanding of the nature of functioning of alive organisms [16–18] provided by this science.

For this aim, it is natural to begin successive analysis of the structurization by plastic flow from very important conclusion of the author [19]: '*Structurization in an open nonlinear medium is associated with the effect of localization*'. It is very important to understand the physical basis of developing synergetic approach to the problem in progress. The use of synergetic principles in plasticity physics requires a more complete than usually description of a deforming medium taking into account such its properties as follow:

- *openness* providing energy inflow from the testing machine to the sample [20];
- *nonlinearity* [21] on the macroscopic level in the form of the strain–stress curve $\sigma(\varepsilon)$ and on the dislocation level in the complex character of the strain–stress interaction during deformation [4–6];
- *inhomogeneity* due to the presence of crystal defects, internal stresses, and other deviations from ideal crystal structure that can lead to self-organization of the structure according to synergetics principles [9–11];
- *activity* of the deforming medium determined by the presence in a media of potential energy sources (elastic stress concentrators) distributed over the volume [5, 18], which can relax during deformation, generating lattice defects;

• *irreversibility* of plastic flow, *i.e.* impossibility of the initial structure restoration after removal of loading because of lattice defect generation [22].

These considerations transfer the deforming media into the class of objects whose properties and dynamics should be described with the help of *the thermodynamic theory of nonequilibrium systems* (*synergetics*) [12–15]. Authors of the monography [13] have declared directly, '*It is impossible to investigate so important and widespread mechanical phenomena as plasticity and yielding on purely mechanical basis; instead, they should be considered as a part of the general subject area of nonlinear dynamic systems operating far from equilibrium*'.

2.2. A Hypothesis about Plastic Deformation Localization

This idea is applicable to plastic deformation during which initially homogeneous medium is spontaneously separated into alternating deforming and nondeforming nuclei whose boundaries can be move. Deformation starts from initiation of the Lüders band [22] on the initial stage of plastic flow and ends by formation of a failure neck directly before a failure. It is reasonable to assume that plastic flow at intermediate stages is localized also macroscopically, and the lack of data is caused by disadvantages of experimental procedures used to record a plastic flow.

These considerations have allowed us to hypothesize that macroscopic localization is a general feature of plastic deformation process accompanying it from elastoplastic transition to failure [23]. Then, the process is characterized shapes of localized plasticity nuclei, rate and character of their motion. Thus, a deformation structure forms in the sense prescribed in [11]; one can suppose that correct explanation of the nature of plasticity is impossible without its analysis.

2.3. Pattern of Plastic Deformation Localization

The hypothesis above has been strongly supported by the results of numerous studies of plastic deformation features in different materials deforming with the help of different microscopic (dislocation) mechanisms. To observe the distribution of localization nuclei on the deforming sample surface, the method combining mechanical tests with double-exposure speckle photography adapted for plastic deformation investigations was used [24, 25]. This allowed the displacement vector field $\mathbf{r}(x, y)$ arising on the flat-sample surface to be reconstructed for step-by-step strain increase by $\delta\varepsilon \approx 10^{-3}$ at any stage of the process. Besides, all the components of plastic distortion tensor

$$\beta_{ij} = \nabla \mathbf{r}\left(x, y\right) = \varepsilon_{ij} + \omega_z = \begin{pmatrix} \varepsilon_{xx} & \varepsilon_{xy} \\ \varepsilon_{yx} & \varepsilon_{yy} \end{pmatrix} + \omega_z \qquad (1)$$

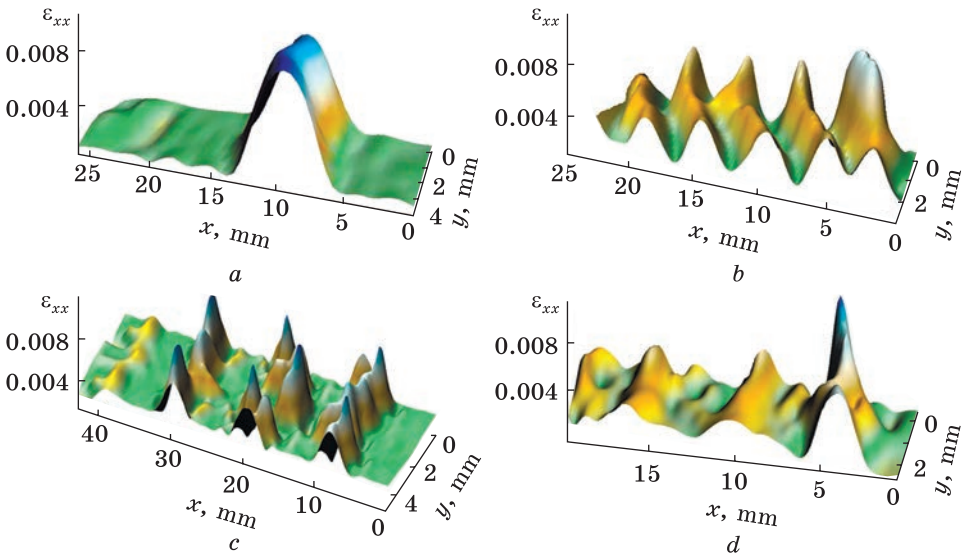

Fig. 1. The examples of localized plastic flow patterns in flat specimens: (*a*) yield plateau in Fe–12 wt.% Mn alloy single crystal; (*b*) linear work hardening stage in polycrystalline Al; (*c*) parabolic work hardening stage in Cu single crystal; (*d*) pre-failure stage in polycrystalline Fe–3 wt.% Si [25]

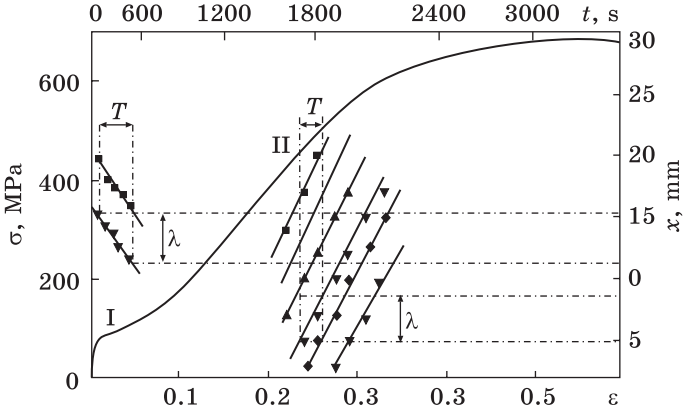

Fig. 2. The example of X–t diagram ant its using for the measurement of spatial, λ, and temporal, T, periods of the localized plastic flow autowave [139]

can be also calculated. Fig. 1, *a*–*d* shows the dependences of the plastic strain tensor component, ε_{xx}, on co-ordinates, x and y in the samples. These dependences are referred as *the localized strain pattern*. The distribution of the tensor components can be analysed using the X–t diagrams, *i.e.* dependences of the strain nucleus co-ordinates, X, on time t. Such diagrams allow to measure the spatial, λ, and temporal, T, periods of the process, as it is shown in Fig. 2. Then the wave number $k = 2\pi/\lambda$, the frequency $\omega = \omega_{aw} = 2\pi/T$, and the motion rate of the deformation nucleus $V_{aw} = \lambda/T = \omega/k$ are calculated.

To elucidate the meaning of the pattern, one can represent the strain increment $\delta\varepsilon$ between two exposures in form

$$\delta\varepsilon \approx \frac{\delta L}{L} \approx \frac{\sum_{i=1}^{N} \left(\varepsilon_{xx}^{(\mathrm{mag})}\right)_i l_i}{L} \approx \frac{N\left\langle \varepsilon_{xx} l \right\rangle}{L}, \qquad (2)$$

where N is the number of localized active flow nuclei with size l in the pattern, $\varepsilon_{xx}^{(\max)}$ is the amplitude of the plastic strain tensor component ε_{xx} in such nuclei, $\langle \varepsilon_{xx} l \rangle$ is the average elongation within the nucleus, and $L > Nl$ is the sample length. Numerical verification of Eq. (2) showed that the total strain is actually the sum of strains in active nuclei, *i.e.* the events in localization nuclei are more essential than the events in the intermediate zones.

A number of authors have independently confirmed the existence of the localized plastic flow pattern (*e.g.*, see the works [26–31]). The used various experimental techniques were based on the laser interferometry, methods of correlation of digital surface images, and the thermovision systems. These investigations have presented the abundant proofs of the correctness of the hypothesis about the universal character of plastic flow localization formulated above.

2.4. Plastic Flow Viewed as Spatial–Temporal Process

After proving the existence of localized plastic flow patterns and determining their temporal dynamics, it became clear that plastic flow is a spatiotemporal process. Immediately, a very important question arose: Can this process be reduced to any already well-known wave process or are we dealings with an unknown regularity of the plasticity phenomenon?

This question arose because, *e.g.*, the Kolsky stress waves are well known. They have been studied theoretically and experimentally in detail in [32, 33]. One can suggest that the Kolsky waves are similar to the discussed deformation processes. However, there are at least three arguments against this. First, the velocity of the Kolsky waves is $10 \le V_{\mathrm{Kol}} \approx (\theta/\rho_0)^{1/2} \le 10^2$ m/s (here, $\theta = d\sigma/d\varepsilon$ is the work hardening coefficient and ρ_0 is the material density) [33]. At the same time, the motion velocity of localized plasticity nuclei is $10^{-5} \le V_{\mathrm{aw}} \le 10^{-4}$ m/s [25]. Evidently, the ratio $V_{\mathrm{Kol}}/V_{\mathrm{aw}} \approx 10^5$–$10^7$ excluded any possibility to reduce the above-discussed localization processes to the Kolsky stress waves. In addition, the velocity V_{aw} cannot be expressed in terms of the material characteristics.

The second argument is the significant difference between the mechanisms of initiation of waves and processes in question. For example, to excite a wave process, an external impact is necessary, whereas a found process is engendered by internal interactions of elements of the active

medium [34]. From representations about the mechanical method of material testing, it is clear that loading is quasi-static in character, so that an external impact is not possible.

Finally, the third argument in favour of the autowave serves limited forms of the stress waves reduced actually only to propagation of solitary fronts [33]. At the same time, the autowaves form different modes [25] corresponding to different experimental patterns of localized plasticity.

Taken together, the arguments presented above allow us to declare that the examined spatiotemporal deformation processes serve as evidence for the existence of a new mechanism of plastic flow. Hähner [35] discussing their nature demonstrated that dislocation responses on the Lüders front are analogous to those observed for the Kolsky stress waves. Simultaneously, in [36] we demonstrated an alternative explanation based on the *autowave processes* [34] arising in active media. Subsequent investigations demonstrated that the autowave theory is preferable for explanation of plasticity features.

Here, it would like to emphasize that the self-organization processes were previously addressed in terms of *dissipative structures* or *pseudowaves* [12, 13] or else as *autowaves* [16]. The latter term needs accurate definition. It is well known [16, 34] that the autowaves are solutions to parabolic differential equations in the partial derivatives, *i.e.*, $\dot{y} = \varphi(x, y) + Dy''$. Similar equations can be produced by adding the nonlinear function $\varphi(x, y)$ to the right-side part of the diffusion equations $\dot{y} = Dy''$. By contrast, hyperbolic differential wave equations of the type $\ddot{y} = c^2 y''$ describe harmonic waves $y \propto \cos(\omega t - kx)$. These waves travel in elastic solids; their rate $c^2 \approx G/\rho_0$ [37] is determined by elastic modulus, G, and the material density, ρ_0.

It is significantly that autowave equations having a first (odd) time derivative, $\dot{y}$, describe irreversible processes, while wave equations having a second (even) time derivative, $\ddot{y}$, cannot be used for the same purpose by virtue of the fact that they have temporal symmetry. Besides, the autowave processes can generate the macroscopic scale due to interaction of microscopic objects. Thus, it is not difficult to appreciate the principal difference between waves and autowaves.

2.5. Pattern; Autowaves; Work Hardening Stages

The correctness of this point of view on the plasticity mechanics was confirmed in Refs. [38–41]. It is important to take into account the geometric meaning of the experimental data: the observable localized plasticity patterns are the cross sections of the volume autowave by the sample surface.

To understand the nature of the phenomenon, as a first step in accomplishing this goal, we compare the patterns of localized plasticity on

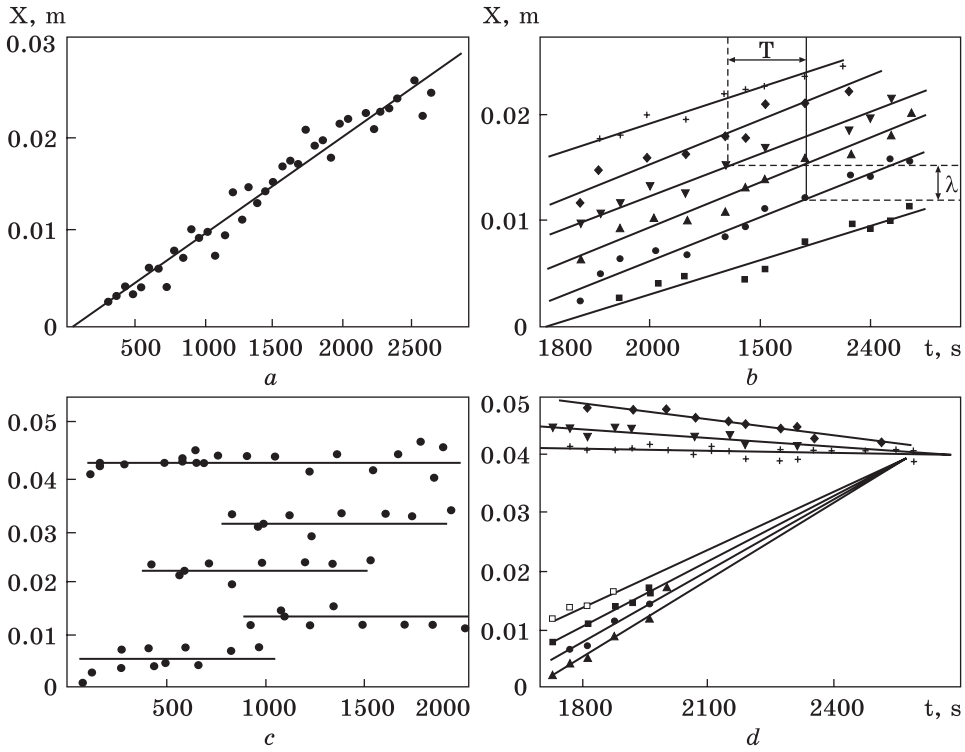

Fig. 3. The correspondence rule. $X-t$ diagrams for (*a*) yield plateau, (*b*) linear work hardening stage, (*c*) parabolic work hardening stage, and (*d*) prefailure stage [25]

different stages of work hardening [5, 6]. These can be seen on the flow curve $\sigma(\varepsilon)$ or on the dependences $\theta(\varepsilon)$ [6, 42]. It turns out that there is a one-to-one correspondence between the work hardening stages and patterns of localization. The $X-t$ diagrams in Fig. 3, *a*–*d* illustrate this clearly.

Thus, at the *yield plateau stage* with $\sigma \approx \text{const}$ and $\theta \approx 0$, the localized plasticity pattern depicts expansion of the single nucleus (Fig. 3, *a*) known as the Lüders band [22]. On its front, the elastic medium is transformed into the plastically deforming the same, changing structure and work hardening law.

At a *linear work hardening stage* when $\sigma \propto \varepsilon$ and $\theta \approx \text{const}$, the hardening is determined by the dislocation interaction and multiplication on dislocation forest [5, 42]. At this stage, the strain pattern is a set of strain nuclei moving equidistantly with a constant rate. In this case, the strain can be repeatedly excited in the same volumes of the material with time intervals determined by the properties and the state of the medium (Fig. 3, *b*).

At a *parabolic work hardening stage* ($\sigma \propto \varepsilon^{1/2}$ and $\theta \propto \varepsilon^{-1/2}$), the process is governed by cross-slip of screw dislocation [4, 42]. A system of

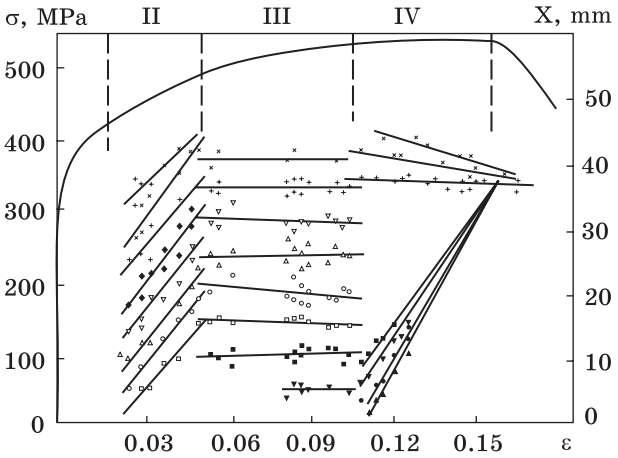

Fig. 4. Successive change of autowave characteristics in the course of plastic flow of polycrystalline Fe–3 wt.% Si alloy [109]

stationary nuclei of plasticity localization (Fig. 3, *c*) is observed in the sample in this case.

At a *prefailure stage* when $\sigma \propto \varepsilon^n$ and $1/2 > n \geq 0$, the strain nuclei move, but the character of the process is more complicated in comparison with the stage of linear work hardening. Here, the time dependences of positions of the localized strain nuclei $X(t)$ are linear and form bunches of straight lines. This is the case at stresses $\sigma_p < \sigma < \sigma_B$, where σ_p is the stress of termination of the parabolic work hardening stage. The velocities of the nuclei in this stage depend linearly on the coordinates of their origin place $\hat{x}$

$$V_{\text{aw}}(\hat{x}) = \alpha_0 + \alpha \hat{x}; \qquad (3)$$

here, α_0 and α are constants. Corresponding X–t diagram is shown in Fig. 3, *d*.

A comparison of the well-known microscopic mechanisms of work hardening at each stage [4–7] with the characteristics of the autowave processes described in [34, 43, 44] allows us to juxtapose a certain autowave mode to each pattern [34] and to formulate the *corresponden-ce rule*:

• at a *yield plateau stage*, the front of localized deformation can be considered as a *switching autowave* of the localized plasticity [34];

• at a *linear work hardening stage*, the *phase autowave* of the localized plasticity is formed [34], for which the condition $\omega t - kx = \text{const}$ is fulfilled; the phase autowave is characterized by the length and oscillation frequency;

• at a *parabolic work hardening stage*, the *stationary dissipative structure* arises [34] arises; in this case the spatial period of the localization nuclei is about the same as the autowave length at the stage of linear work hardening;

• at a *prefailure stage*, it is observed the *collapse of the autowave process* of localization [45] before the failure neck formation.

The correctness of the correspondence rule is illustrated by Fig. 4 on the example of the deformation of polycrystalline Fe–3 wt.% Si alloy. However, it is necessary to emphasize that the Correspondence rule is fulfilled independently on the investigated material nature and structure [25]. As was found, there are four major autowave modes, which can arise in the course of plastic flow. They unambiguously correspond to the work hardening stages, and the plastic flow can be considered as the sequence of the autowave modes strongly determined by the acting laws of work hardening. This observation led to the following interesting consequence. As well known, significant alterations of autowave modes can be observed and modelled in chemical and biological systems too [34]. However, autowave generation in similar systems requires special generators for each mode. Indeed, a metal sample of simple shape in tension with a constant velocity at a constant temperature can spontaneously generate autowaves of different types caused by transformations of defect structure. It is conceivable that the deforming sample can be considered as a universal generator of different autowave modes [46].

2.6. Experimental Data on the Phase Autowaves of Localized Plastic Flow

The phase autowaves of the localized plasticity are most convenient and interesting for he detailed analysis since their lengths and propagation velocities have been measured sufficiently precisely. Empirical features have been established for them, including the dependence of the propagation velocity on the work hardening coefficient $V_{aw}(\theta)$, the dispersion law $\omega(k)$, and the dependence of the length of autowave on the grain size $\lambda(\delta)$.

At the easy slip in single crystals and linear work hardening stages, this dependence is shown in Fig. 5, *a*. Obviously,

$$V_{aw}(\theta) = V_0 + \frac{\Xi}{\theta} \propto \theta^{-1}, \tag{4}$$

where V_0 and Ξ are constants, different for easy glide and linear work hardening stages. The correlation coefficients between V_{aw} and θ^{-1} at these stages are ≈0.7 [47]. The proportionality $V_{aw} \propto \theta^{-1}$ confirms some more the difference between the localized plasticity autowaves and the Kolsky waves [32], for which $V_{Kol} \propto \theta^{1/2}$.

As shown experimentally [48, 49], the dispersion law for localized plastic flow autowaves has the quadratic form (Fig. 5, *b*)

$$\omega = \omega_{aw} = \omega(k) = \omega_0 + \alpha(k - k_0)^2, \tag{5}$$

where a, k_0, and ω_0 are constants depending on the material. By substitutions $\omega = \omega_0\tilde{\omega}$ and $k = k_0 + \tilde{k}/\sqrt{\alpha/\omega_0}$, where $\tilde{\omega}$ and $\tilde{k}$ are dimensionless frequency and wave number, Eq. (5) is reduced to its canonical form $\tilde{\omega} = 1 + \tilde{k}^2$. It is of importance that similar dispersion law is typical for

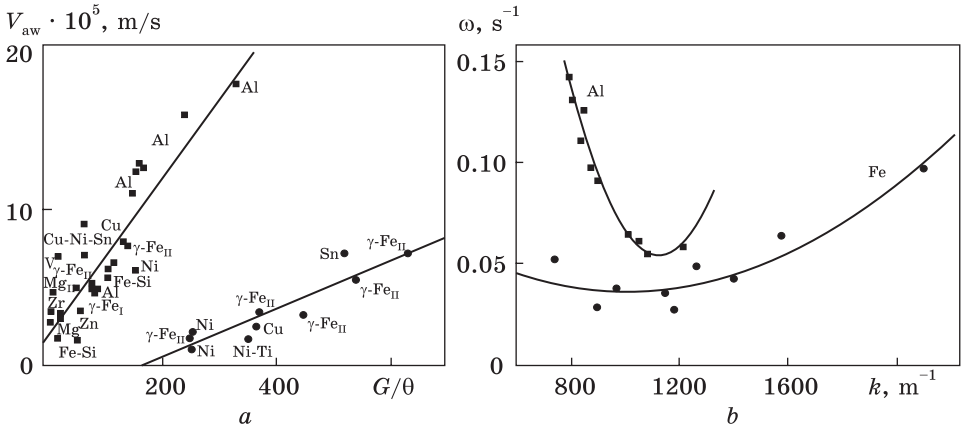

Fig. 5. Characteristics of phase autowaves: *a* — the rate of localized plastic flow autowaves as a function of work hardening coefficient for linear work hardening (upper curve) and easy glide (lower curve) [49]; *b* — dispersion law for localized plastic flow autowaves [48]

many nonlinear processes developing in the non-equilibrium systems of different kinds [21, 34].

There is a gap in the dependence $\omega(k)$ at $0 \le \omega < \omega_0 \approx 10^{-2}$ Hz (see Fig. 5, *b*). Therefore, the condition $\hbar\omega_0 \ll k_B T$ is fulfilled at any temperature, and spontaneous localization of the plastic flow can be excited in all these cases. Thus, *e.g.*, the jump-like strain associated with localization was observed at $T \le 1$ K [50]. Probably, the plastic strain localization autowaves can be absent only because of geometrical restrictions for small sample sizes [12].

This dependence was established for polycrystalline Al [51] with grain sizes $5 \cdot 10^{-6} \le \delta \le 5 \cdot 10^{-3}$ m that were prepared by recrystallization at 853 K after deformation. The dependence $\lambda(\delta)$ is shown in Fig. 6. When choosing the form of the function $\lambda(\delta)$, it was taken into account that the localized strain wavelength increased with elongation of the shear lines. If the grain size becomes close to the sample size, the rate of growth slowed down, because the length of the slip line cannot exceed the grain size. Hence, it follows that $d\lambda/d\delta = a\lambda - a^*\lambda^2$, where $a > 0$ and $a^* > 0$ are dimensional constants, and the term $a^*\lambda^2$ takes into account slowing down of the λ increment at large δ. Integration of this equation yields the Ver-

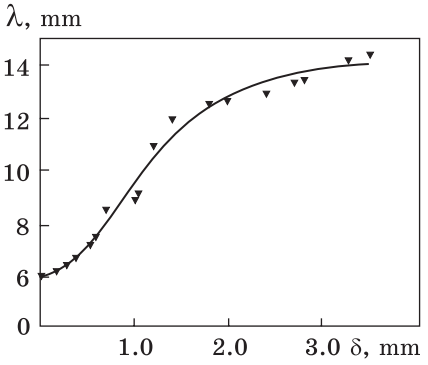

Fig. 6. Length of autowave as a function of grain size (polycrystalline Al) [51]

hulst (logistic) function [12]:

$$\lambda = \lambda_0 + \frac{\lambda^*}{1 + C\exp(-a\delta)}, \qquad (6)$$

where $C \approx 2.25$ and the constants $\lambda_0 \approx 4\cdot10^{-3}$ m, $a = 1.4\cdot10^{3}$ m^{-1}, $a^* = 8.8\cdot10^{4}$ m^{-2}, and $\lambda^* = a/a^* \approx 1.6\cdot10^{-3}$ m were determined experimentally.

3. Plastic Flow Localization: Quantitative Analysis

As shown above, the autowave processes are described by differential equations of type $\dot{y} = \varphi(x, y) + Dy''$ [34, 43, 52]. An explicit form of the function $\varphi(x, y)$ is determined by physical reasons either if the mechanism of the phenomenon is known or is written in the form of cubic nonlinearity. Methods of solving these equations [54] have been successfully used to analyse the dynamics of structures in chemical and biological objects.

However, actual models of autowave processes are based on a competition of the autocatalytic (activator) and damping (inhibitor) factors that govern the kinetics of the corresponding process [13, 34, 53]. For this reason, we need two equations to describe adequately the plasticity phenomena. This problem is simple, *e.g.*, for chemical kinetics: one of the equations describes the activator concentration and another describes the inhibitor concentration. In systems of other nature, the choice of the governing factors is a more complicated problem.

3.1. Autowave Equations of Plastic Flow

The complexity of physical aspects of the plasticity problem consists in optimal choice of variables suitable for a description of plastic flow processes. For a localized plastic flow, it was suggested to consider the plastic strain ε as an activator and the elastic stress σ as an inhibitor of the process [25]. The main argument in favour of such choice is as follows. As we know [2, 55], to describe the plastic deformation of a solid, the stress tensor is subdivided into the deviator stress tensor and spherical the same. In this case, the deviator stress tensor is responsible for plastic change of the form, and the spherical tensor creates hydrostatic compression or tension that prevents the plastic strain according to the law of elasticity of volume strain [2]. The choice of the plastic strain and elastic stress as control parameters is convenient because it allows experimental determination of σ and ε from the diagram $\sigma(\varepsilon)$ and spatial separation of elastically stressed and plastically strained zones defining the multiscale character of the process [56].

The evidences in favour of such choice are adiabatic cooling of the sample in tension and local heat liberation in shear planes [10]. These

processes are opposite. Authors [57] hold a similar point of view on the nature of the activator and inhibitor of plastic deformation. Taking into account this choice, the equations for the strain (activator) and stress (inhibitor) can be written by analogy with [34, 53] (they are actually postulated) in the form of the system of equations

$$\begin{cases} \dot{\varepsilon} = f(\varepsilon) + D_{\varepsilon\varepsilon}\varepsilon'', & (7) \\ \dot{\sigma} = g(\sigma) + D_{\sigma\sigma}\sigma'', & (8) \end{cases}$$

where the first equation describes the kinetic strain changes (activator), and the second equation describes the stress (inhibitor). Double subscripts of the coefficients $D_{\varepsilon\varepsilon}$ and $D_{\sigma\sigma}$ in Eqs. (7) and (8) are explained below.

The nonlinear functions $f(\varepsilon)$ and $g(\sigma)$ describe the relaxation events on the strain fronts in nonlinear deforming medium [5, 58]. They characterize the redistribution of strains and stresses among neighbouring microvolumes near the relaxing stress concentrator and are due to continuous motion of the strain front.

The diffusion terms $D_{\varepsilon\varepsilon}\varepsilon''$ and $D_{\sigma\sigma}\sigma''$ determine the macroscale redistribution of the strain and stress. Thus, one can consider that the right sides of Eqs. (7) and (8) contain *hydrodynamic* ($f(\varepsilon)$ and $g(\sigma)$) and *diffusion-like* ($D_{\varepsilon\varepsilon}\varepsilon''$ and $D_{\sigma\sigma}\sigma''$) components [59]. The roles of the hydrodynamic and diffusion-like components in the strain dynamic development are different essentially.

As follows from the theory of parabolic differential equations [43], the interaction propagation rate in medium is infinite, *i.e.*, $V^{(\text{inter})} \to \infty$. Such condition is physically unrealizable and must be replaced by the condition $V^{(\text{inter})} \approx V_t$ that limits the velocity of signal transfer in the medium by the sound velocity, V_t. On this reason, the time of emergence of new plasticity nucleus is $\tau \geq \lambda/V_t$. This one gives rise to the idea that the acoustic properties of the medium can play an important role in the initiation of new dislocation shears at a macroscopic distance from the existing plasticity nucleus [60]. We note also that the first-order time derivatives in Eqs. (7) and (8) emphasize the irreversible, in principle, character of plastic flow. Thus, Eqs. (7) and (8) take into account *nonlinearity* and *activity* of the deforming medium as well as the *openness* of the system and the *irreversibility* of the plastic flow.

Equations (7) and (8) have to be derived from the master equations of mechanics. Thus, *e.g.*, Eq. (7) follows from the condition of continuity of functions describing deformation kinetics [61]. In this case,

$$\dot{\varepsilon} = \nabla \cdot \left(D_{\varepsilon\varepsilon}\nabla\varepsilon\right), \quad (9)$$

where $D_{\varepsilon\varepsilon}\nabla\varepsilon$ is the strain flow in the field of its gradient. If $D_{\varepsilon\varepsilon} = D_{\varepsilon\varepsilon}(x)$, then

$$\dot{\varepsilon} = \varepsilon' \cdot D'_{\varepsilon\varepsilon} + D_{\varepsilon\varepsilon}\varepsilon'' = f(\varepsilon) + D_{\varepsilon\varepsilon}\varepsilon'', \quad (10)$$

where $f(\varepsilon, \sigma) = \varepsilon' \cdot D'_{\varepsilon\varepsilon}$ is a nonlinear function of the strain and stress. It is clear that Eq. (10) is equivalent to Eq. (7) postulated above.

In its turn, Eq. (8) follows from the Euler equation [62],

$$\frac{\partial}{\partial t}\rho v_i = -\frac{\partial \Pi_{ik}}{\partial x_k}, \tag{11}$$

where $\Pi_{ik} = p\delta_{ik} + \rho v_i v_k - \sigma_{\text{vis}} = \sigma_{ik} - \rho v_i v_k$ is the momentum flow density tensor, δ_{ik} is the unit tensor, p is the pressure, and v_i and v_k are the components of the flow velocity. The stress tensor $\delta_{ik} = -p\delta_{ik} + \sigma_{\text{vis}}$ is the sum of elastic, $\sigma_{\text{el}} = -p\delta_{ik}$, and viscous, σ_{vis} stress components, that is, $\sigma = \sigma_{\text{el}} + \sigma_{\text{vis}}$, and $\dot{\sigma} = \dot{\sigma}_{\text{el}} + \dot{\sigma}_{\text{vis}}$. Here, $\dot{\sigma}_{\text{el}} \equiv g(\sigma, \varepsilon) = -B^{-1}M\rho_d b^2\sigma = -M\rho_m b V_{\text{disl}} \propto V_{\text{disl}}$, where M is the elastic modulus of the sample, $B \approx 10^{-5}$–10^{-4} Pa·s is the dislocation drag coefficient, and $V_{\text{disl}} = (b/B)\sigma$ is the dislocation rate [50, 63].

The viscous stresses depend on the elastic wave velocity in the medium and its dynamic viscosity η: $\sigma_{\text{vis}} = \eta\nabla V_t$; here, $V_t \approx V_{t_0} + \beta\sigma$ [60], V_{t_0} — propagation velocity of the transverse elastic waves at $\sigma = 0$ and $\beta = \text{const}$. In this case, $\partial\sigma_{\text{vis}}/\partial t = V_t\nabla\cdot(\nabla V_t) = \eta V_t\partial^2 V_t/\partial x^2$, and the relaxation rate of viscous stress is $\partial\sigma_{\text{vis}}/\partial t = \eta V_t\partial^2 V_t/\partial x^2 = \eta\beta V_t\partial^2\sigma/\partial x^2$, so that

$$\partial\sigma/\partial t = g(\sigma) + D_{\sigma\sigma}\,\partial^2\sigma/\partial x^2\,, \tag{12}$$

where $D_{\sigma\sigma} = \eta\beta V_t$ is the transfer coefficient. Thus, the terms $\dot{\sigma}_{\text{el}} = g(\sigma)$ and $\dot{\sigma}_{\text{vis}} = D_{\sigma\sigma}\,\partial^2\sigma/\partial x^2$ in Eq. (12) determine the relaxation rates of the elastic and viscous stresses, respectively, and Eqs. (12) and (8) are equivalent.

3.2. Analysis of the Autowave Plasticity Equations

To estimate the possibilities of Eqs. (7) and (8) for a description of localized plasticity, we now consider the explicit form of the nonlinear functions:

$$f(\varepsilon) = -\frac{\varepsilon}{\theta_\varepsilon} + \frac{\sigma}{\eta} \tag{13}$$

and

$$g(\sigma) = -\frac{(\sigma - \sigma_y) - \sigma^*}{\theta_\sigma} + \frac{\sigma\varepsilon}{\theta_\varepsilon}, \tag{14}$$

where η is the viscosity of the medium, θ_ε and $\theta_\sigma << \theta_\varepsilon$ are the relaxation times of the strain and elastic stresses, and σ_y is the yield strength. Equation (13) is the Maxwell equation for a viscoelastic medium. The first term in Eq. (14) describes the stress relaxation to the level σ^*, and the second term describes the nonlinear feedback effects.

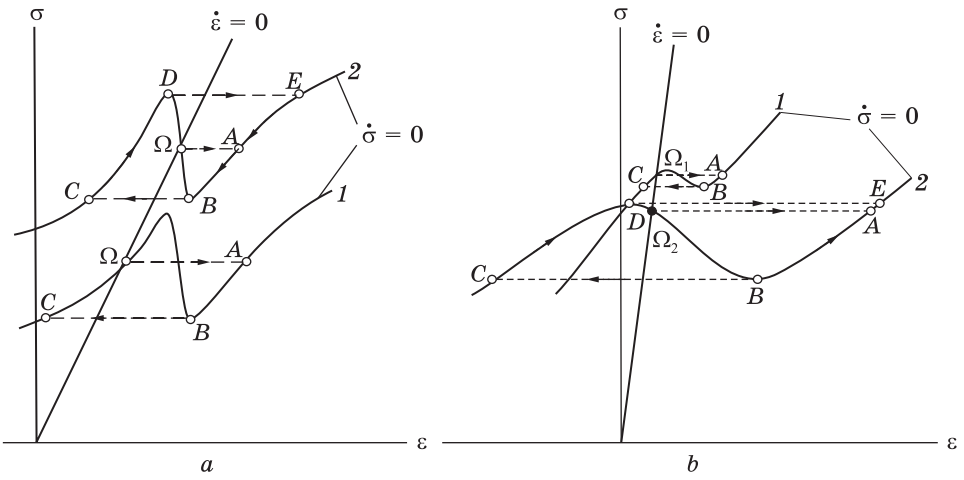

Fig. 7. 0-isoclines corresponding to Eqs. (15) and (16) (*a*) as well as (18) and (15) (*b*) [41]

To analyse qualitatively Eqs. (13) and (14), we take advantage the method isoclinic lines for what equate to zero the left-side sides of the equations. Then,

$$\sigma = \frac{\eta}{\theta_\sigma}\varepsilon = G\varepsilon \tag{15}$$

and

$$\sigma = \frac{\sigma_0 + \sigma_y}{1 - (\theta_\sigma/\theta_\varepsilon)\varepsilon}. \tag{16}$$

The 0-isoclinic lines so obtained are shown in Fig. 7, *a*. Their analysis consists of the search of intersection points for 0-isoclinic lines. The *N*-shaped form and the position of function (16) are determined by constants entering into it and by the strain ε. For small stresses, after achievement of the special point Ω, any small deviation from the equilibrium leads to the jump-like transition $\Omega \to A$ to the stable isoclinic line branch $\dot{\sigma} = 0$. At low stresses, the point makes the cycle $A \to B \to$ $\to C \to \Omega$, and the system returns to the equilibrium again. At high stresses (the upper curve), after disruption of the equilibrium $\Omega \to$ A, the depicting point no longer returns to the equilibrium position and moves along the closed trajectory $A \to B \to C \to D \to E \to B$. The first case corresponds to the propagation of the switching autowave (the Lüders front). The repetition of cycles in the second case indicates the formation of the phase autowave.

The function $f(\varepsilon)$ can also be defined in another way. For example, for the thermal activation character of the relaxation process, this de-

pendence can be logarithmic in character, which follows from the kinetics of the thermally activated plastic deformation [64]. Then

$$f(\varepsilon) = \frac{A}{\theta_\sigma} \ln \varepsilon + \frac{\sigma - \sigma_\vartheta}{\theta_\sigma}, \tag{17}$$

where the constant A is determined by the mechanism of plastic strain and σ_ϑ is the stress function. The equation for the 0-isoclinic line in this case has the form

$$\sigma = \sigma_\vartheta + A \ln \varepsilon \tag{18}$$

shown in Fig. 7, *b*. The subsequent analysis also demonstrates the change in plastic flow modes. At low stresses (curve *1*), the depicting point on the path $\Omega_1 \to A \to B \to C$ returns to the equilibrium position. At high stresses (curve 2), the depicting point after transition $\Omega_2 \to A$ moves along the trajectory $B \to C \to D \to E \to B$ that corresponds to the formation of the phase autowave.

Thus, Eqs. (7), (8), (10), and (12) are applicable for a description of the autowave phenomena at the plastic flow. With their use, the existence of switching and phase localized plasticity autowaves at stages of the yield plateau and linear work hardening, respectively, can be explained.

3.3. On the Application of the Autowave Representations

One of the first attempts to use Eq. (7) in physics of lattice defects belongs to Donth [65, 66] who explained with its help the contribution of dislocation kink motion to the amplitude-dependent internal friction. Later on, such ideas were used directly to describe the self-organization of dislocation ensembles during plastic deformation. For example, the situation with propagation of strain fronts was studied in [67, 68], where correct estimation was obtained of the autowave propagation velocity of inhomogeneous plastic shear (the switching autowave) for motion of the Lüders band.

In Refs. [69–72], the autowave representations were used to solve the problem of the jump-like strain and to analyse the formation of slip bands. For these purposes, the authors wrote dynamic equations for dislocation ensembles and considered conditions of forming slip bands from originally chaotic defect distribution. The complex structure of the strain waves propagating in the deforming medium and consisting of the head part of soliton type and of the oscillating tail gradually lagging behind the head part during motion was predicted. This effect can be considered as one of the mechanisms of autowave generation in deforming media. General analysis of the stability problem for a dislocation ensemble demonstrated that dislocation density fluctuations lead to the emergence of stress concentrators in a deforming medium.

Apparently, the mechanisms of self-organization and formation of dislocation ensembles were considered most consistent and rigorously in [73–76]. Thus, in [74] the relationship between the strength and plasticity was analysed on the examples of work hardening curves for some f.c.c. metals and alloys. The analysis was based on the neck formation criterion in a sample in tension and on the work hardening curve elated to dislocation density in the material with increasing strain degree and the influence of structural factors on this dynamics.

The influence of the Peierls stress on both the stress and the strain before the neck formation was studied in Ref. [75] for metals in tension. The analysis was based on the dependence of dislocation density on strain in the course of the material work hardening and the influence of the Peierls stress on this process in terms of the screw dislocation annihilation. In Ref. [76], the mechanism of work hardening and dislocation structure fragmentation in metals subjected to severe plastic deformation was explained on the base on the dislocation kinetics equations.

The important attempts to explain the autowave processes of plastic flow were undertaken by the authors [77, 78]. To analyse the situation, they represented the total local strain of the medium in the form of a sum of elastic, irreversible inelastic and reversible inelastic terms. Since the inelastic strain is of the localized type, quantities and can be written using the order parameters q and $p < q$, which define the fractions of the volume occupied by reversible and irreversible inelastic deformation zones, respectively. Variables $p(r, t)$ and $q(r, t)$ characterizing the variation of the internal structure of the strained material will be hence forth treated as the Landau order parameters and are assumed to be continuous functions of co-ordinates and time. Clearly, $0 \le q \le 1$ and $0 \le p \le 1$; for $q = 0$ and $p = 0$, the sample experiences only elastic deformation, while for $q > 0$ and $p > 0$, the sample is under uniform inelastic strain.

These representations are generalizations of the equations describing self-organization processes in active media [12, 13] to the case of a deformable medium. The change in the state of the medium under plastic deformation is determined by the matched redistribution of elastic stresses and the motion of localized plasticity zones emerging at any stage of the process.

Thus, the authors of [77, 78], based on the autowave approach, succeeded in explaining the transition of the autowave strain modes to the plastic flow from the Lüders front to the phase autowave and the quadratic dependence of the autowave dispersion at the stage of linear work hardening stage.

In works [79, 80], it was considered the possibility of self-organization of dislocation structures at a plastic flow by the introduction of the

hydrodynamic strain flow component, and showed how such process affects the work hardening. They demonstrated that the deformation process dynamics obeys the synergetic laws.

4. Generation of Plastic Strain Autowaves: A Model

A role of the strain, ε, and stress, σ, governing the plastic flow, can be the following. The autocatalytic factor (strain) acts so that each accomplished shear initiates the similar process in the neighbouring volume required for accommodation, so that the effective radius of action for this parameter is on the order of the shear zone size, l, and its propagation velocity is commensurable with the dislocation velocity, V_{disl}. The elastic energy released during each shear is redistributed within the volume, causing relative growth of the stress concentration, which damps the plastic strain. The radius of action of this factor is commensurable with the sample size $L >> l$, and the propagation velocity is equal to that of the elastic waves $V_t >> V_{\text{disl}}$. Such relationship for the activating and inhibiting factors that governs the process is necessary for autowave generation [34].

4.1. Plastic Flow as a Self-Organization Process in a Deforming Medium

Haken [15] was the first who stated, '*The system is called self-organizing if it acquires any spatial, time, or functional structure without specific external impact*'. From this point of view, spontaneous stratification of the medium during plastic flow into deforming and non-deforming volumes is equivalent to its self-organization that is, ordering (structurization). A description of such processes is a main problem of synergetics.

Olemskoi and co-authors in [14, 81–83] applied synergetic apparatus to a detailed description of problems of condensed state physics, including the plastic flow and failure questions. In particular, he first succeeded in consideration from these positions the patterns of formation of crystal defects and autowaves related to the localization of plastic flow in the condition of active loading and at the phase transformations.

In the works [84–91], problems of condensed media structurization were analysed, in particular, for the formation of localized plasticity autowaves and the nature of hydrodynamic and diffusion-like plastic flow modes. The application of these ideas directly to a solution of the plasticity problem signalled a new look on the plastic strain as on the process of self-organization of defective structure on different scale levels. Author [84, 85] successfully used the synergetic approach to describe the strain nature and the destruction processes based on excitation mechanisms of the crystal lattice. In Refs. [86–91], the authors

described the process of plastic strain as a non-equilibrium kinetic transition leading to plastic flow localization. Within the framework of this approach, the deforming material was considered as a system capable of generating dissipative structures more efficient in comparison with motion of single dislocations, in particular, plastic flow autowaves. This is in agreement with the results of investigations of dislocation structures in a plastic flow. Thus, for example, authors of work [92] established and discussed regularities of generation of new dislocation substructures during deformation and showed that a new structure emerges against the background of the old structure and is accompanied by its degradation.

4.2. Autowave Plastic Flow Model

The new approach required the development of a self-organization model focused on the problem of plasticity of solids. For this aim, the idea was used moved by Kadomtsev [45] who considered that '*During self-organization of complicated open physical systems, trends may emerge toward their stratification into information and dynamic subsystems*'.

This claim is in full agreement with representations about competition between the autocatalytic and damping factors discussed above, and a relationship can be seen of the dynamic and information subsystems with them. Therefore, to develop a model, we define the specificity of the information and dynamic subsystems in a deforming medium bearing in mind that:

- the origin of the information and dynamic subsystems should be closely related to the processes that control the plastic flow;
- there should be a mechanism of subsystem interaction of such power that events in one subsystem could cause responses in another.

Total deformation involves the both elastic and plastic components. The elastic state at nominal stresses $\sigma_{\text{nom}} < \sigma_y$ is characterized by the presence in the material of a set of dwelling stress concentrators with amplitude $\sigma_c \gg \sigma_{\text{nom}}$ randomly distributed over the volume, which is typical of an active medium. For $\sigma_{\text{nom}} > \sigma_y$, the medium is transformed into the plastic state, in which a part of the concentrators remains in the dwelling state, and another part relaxes. This is taken into account in the *two-component plasticity model*, the flowchart of which is shown in Fig. 8, *a*. In this case, *the dynamic subsystem* is formed by a set of relaxing concentrators — elementary plastic strain relaxation events. Here thermally activated relaxation (destruction) of the concentrator is considered as an elementary plastic flow event of dislocation shear, twinning, *etc*. *The information subsystem* includes a set of elastic pulses of acoustic emission generating and absorbing by relaxation events.

The state of a deforming medium in this model is characterized by wandering of acoustic pulses in the system of elastic stress concen-

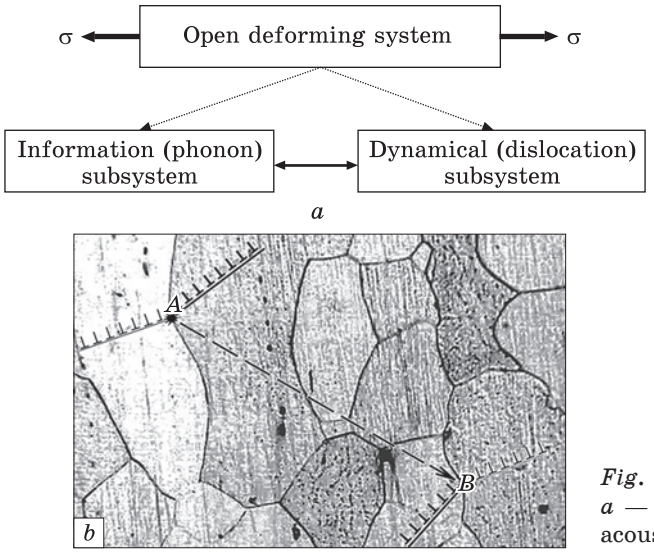

Fig. 8. Two-component model: *a* — flowchart; *b* — mechanic-acoustic scheme [38]

trators. Being superimposed on the elastic concentrator fields, they trigger plastic strain relaxation events. Autowave are generated due to interaction of the dynamic and information subsystems provided on the one hand, by generation of pulses of acoustic emission in each relaxation event, and on the other hand, by their absorption by dwelling concentrators. Thus, either *spontaneous* or *induced* relaxation acts are observed in the deforming system for the condition $\sigma_{nom} < \sigma_y$; the latter activate waiting concentrators again by acoustic emission pulses [93–95].

The scenario of plastic flow shown in Fig. 8, *b* includes the two steps. First, transformations in the dynamic subsystem, that is, spontaneous or induced plastic shear (transformation of the dwelling concentrator into the relaxing one and again into the dwelling one; points *A* and *B*). After that, transformations in the information subsystem, that is, emission of acoustic pulse in the process of concentrator destruction (point *A*) and its absorption by another waiting concentrator (point *C*). Then these acts are repeated.

Thus, two effects, typically studied separately, are combined in the two-component model. The first effect is the acoustic emission accompanying the plastic flow events and conventionally used to control the material state [93, 96]. The second effect is acoustoplasticity whose mechanism, explained in works [94, 95], consists in plasticization of the material by imposing of stress oscillations with ultrasonic frequency on a deforming material.

Obviously, the above-described mechanism is possible because of the known property of a nonlinear deforming medium to generate harmon-

ics during elastic signal propagation. In this case, the elements of the medium can be related with these harmonics [45]. Thus, in particular, if the acoustic signal containing the harmonic of a certain frequency is generated in the process of destruction of the stress concentrator A, such harmonic can be absorbed by the accepting concentrator C of similar structure and spectrum with the corresponding increase of the impact. It is possible to add that the generation of harmonics is a consequence of nonlinearity of deforming medium.

4.3. Quantitative Estimations of the Model

Let us compare the waiting times of thermally activated relaxation events [64] in the absence of acoustic pulse (spontaneous relaxation)

$$\vartheta_{\text{sp}} \approx \omega_D^{-1} \exp\left(\frac{U_0 - \gamma\sigma}{k_B T}\right), \tag{19}$$

and after pulse imposition (induced relaxation)

$$\vartheta_{\text{ind}} \approx \omega_D^{-1} \exp\left[\frac{U_0 - \gamma\sigma - \delta U_{\text{ac}}}{k_B T}\right] \approx \omega_D^{-1} \exp\left[\frac{U_0 - \gamma\left(\sigma + \varepsilon_{\text{ac}} E\right)}{k_B T}\right]. \tag{20}$$

In Eqs. (19) and (20), ω_D is the Debye frequency, U_0 is the potential barrier to be overcome during the relaxation event, $\gamma \approx b^2 l \approx 10^4 b^3$ is the activation volume of this event [64], l is the size of the shear zone, k_B is the Boltzmann constant, T is temperature, and E is the elastic modulus. In calculations by formulas (19) and (20), we set that the activation enthalpy of the destruction process is $U_0 - \gamma\sigma \approx 0.5$ eV, and the acoustic pulse with elastic strain amplitude ε_{ac} decreases this parameter by $\delta U_0 \approx \gamma\varepsilon_{\text{ac}} E \approx 0.1$ eV. Calculation for $k_B T \approx 1/40$ eV yields $\vartheta_{\text{sp}} \approx 5 \cdot 10^{-5}$ s and $\vartheta_{\text{ind}} \approx 9 \cdot 10^{-7}$ s $\ll \vartheta_{\text{sp}}$. Such estimations explain the possibility of plastic flow activation under the action of acoustic pulses and confirm the correctness of the model.

Thus, Eqs. (19) and (20) demonstrate the possibility of induced decay of stress concentrator fields. It seems likely that the rate of localized plasticity autowave is determined by the time of plasticity nucleus growth from a nucleus that can be identified with the intergrowth of the Lüders band through the sample ($\tau L \approx 10$ s $\gg \vartheta_{\text{sp}}$, Fig. 9).

The principal problem in explanation of the autowave nature irrespective of the system nature is matching of the macroscopic autowave scale with the microscale of internal interactions. In the context of the model being developed, it can be explained as follows. Let a shear emits a pulse of transverse acoustic waves with frequency $\omega_m \approx 10^6$ Hz corresponding to a maximum of the spectrum [93]. As shown in [97], having passed through an elastically stressed region, such pulse is split into

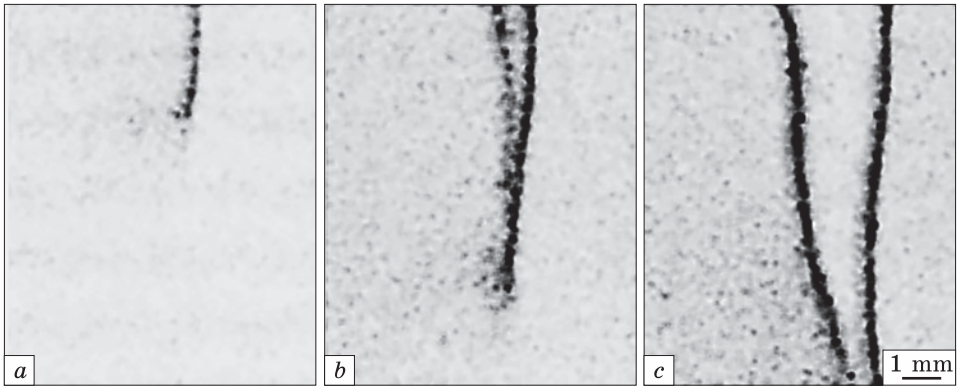

Fig. 9. Increase of the Lüders band across deforming sample. Time between frames is 7 s [25]

two orthogonally polarized acoustic waves propagating with velocities v_1 and $v_2 \neq v_1$. The difference between their wavelengths

$$\delta L = L_2 - L_1 \approx \frac{v_2 - v_1}{\omega_m} \approx \frac{\sigma_2 - \sigma_1}{2\omega_m \rho_0 V_t} \qquad (21)$$

reaches $\sim 10^{-4}$ m provided that the difference between the principal normal stresses $\sigma_2 \approx \sigma_2 \approx 10^2$ MPa in Eq. (21), the material density $\rho_0 \approx 5 \cdot 10^3$ kg/m^3, and the sound velocity $V_t \approx 10^3$ m/s. The probability of activation of a new shear increases when the maxima of σ^2 coincide in both waves, that is, when the elastic energy is maximal. This corresponds to the condition $L^2/\delta L \approx \lambda \approx 10^{-2}$ m, which is close to the observable autowave length and explains the origin of the plasticity nuclei at the distance $\sim\lambda$ from the existing strain front at the expense of the process of acoustic initiation of strain.

Another variant of estimation is based on an analysis of acoustic signal propagation through a fragment with inhomogeneous density of dislocations of the type of the existing plastic flow nucleus (Fig. 10, *a*). If the dislocation density in the fragment decreases from the nucleus toward the periphery, the internal stresses $\sigma_i \approx Gb\rho_d^{1/2}$ [6] are inhomogeneously distributed. Such fragment can be considered as an acoustic lens with diameter C. Together with the dependence $V_t \propto \sigma_i$ [60], this causes rotation of the plane wave front A–A passing in this region through a small angle α.

The waves from neighbouring regions playing the role of lenses are focused onto the symmetry axis where the level of the elastic stress increases, thereby increasing the probability of relaxation plasticity events. This initiates the formation of a new strain nucleus at the distance $\sim\lambda$ from the initial nucleus. Simple geometric calculation the

details of which and the designations are explained in Fig. 10, *a* demonstrates that

$$\lambda \approx \frac{C}{2\sin\alpha} \approx \frac{C}{2\tan\alpha} \approx \frac{1}{\Delta V_t \delta / CV_t} \approx C\frac{C}{2\delta}\frac{V_t}{\Delta V_t}. \qquad (22)$$

It is convenient to estimate the effect quantitatively for polycrystalline Al in which the velocity is $V_t \approx 3\cdot 10^3$ m/s, and its experimentally determined range of variation in the plastic strain interval corresponding to the parabolic work hardening stage is $\Delta V_t \le 10$ m/s [60]. For the fragment size $\delta \approx 10^{-7}$ m and the ratio $C/2\delta \approx 10$, we obtain $\lambda \approx 10^{-2}$ m, which is close to the observable distance between the localized strain nuclei (autowave strain length). Since $\lambda \gg C > b$, we can consider that Eq. (22) relates the microscale of the dislocation substructures and the macroscale of the autowave deformation.

A simpler variant of such estimation is possible. Since the velocity of elastic waves depends on the strain and the dislocations are conventionally distributed inhomogeneously. The inhomogeneity zone with size l_d can be considered as an acoustic lens with curvature radius $R \approx l_d$. Its focal length ξ (Fig. 10, *b*) is [49]

$$\xi = \frac{R}{\kappa - 1}, \qquad (23)$$

where $\kappa = V_0/V$ is the refractive index of sound waves in the defor-ming medium. From experimental data presented in Ref. [60], it follows

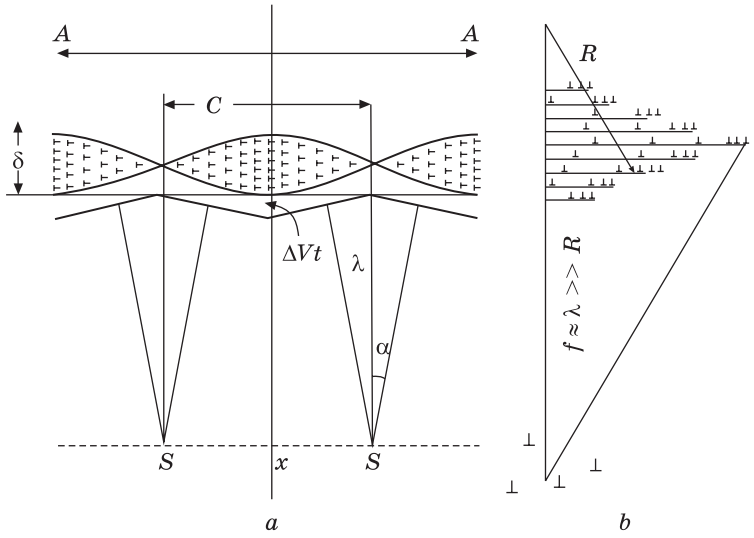

Fig. 10. Dislocation structure inhomogeneities viewed as (*a*) acoustic lenses scheme for calculations, and (*b*) its simplified variant [121]

that $\kappa \leq 1.002$ almost until destruction; during deformation of Al, $R \approx l_d \approx 10^{-5}$ m. Then, according to Eq. (23), $\xi \approx \lambda \approx 5 \cdot 10^{-3}$ m. The probability of stress concentrator destruction increases at this distance, and a new strain localization nucleus is formed. Since the parameters κ and R are determined by the material structure, the dynamics of the strain nuclei in the plastic flow can control reorganization of the autowave strain localization pattern. Dislocation ensembles with inhomogeneous distribution of defects, — dislocation chaos, cells, *etc.*, — can play the role of acoustic lenses [4, 7, 98].

In these cases, variants of propagation and behaviour of macroscopic localized strain zones can be caused by the change of the acoustic lens geometry (parameters C and δ and their ratio $C/2\delta$) or dislocation distributions during plastic flow. According to Eq. (22), the increase of fragment size initiates growth of λ and can cause motion of the plastic flow nucleus along the tension axis at the stage of linear work hardening.

The above estimations point out the possible solution of the most complicated problem of physics of plasticity. It is emergence of macroscopic autowave scale of $\sim 10^{-2}$ m in deforming material whose structural defects (dislocations) have spatial scale on the order of the Burgers vector of $\sim 10^{-10}$ m. It is not difficult to see that the two-component plasticity model accounts well such values.

5. Elastic–Plastic Strain Invariant

The principal role in the two-component model of localized plasticity is played the interaction of elastic waves with plastic shears directly in the process of changing the form. The existence of the quantitative relationship between the corresponding characteristics was established using the numerical analysis of quantitative data of the localized plastic flow dynamics.

5.1. The Acceptance of the Elastic–Plastic Strain Invariant

For phase autowaves of localized plasticity, the relationship

$$\frac{\lambda V_{\text{aw}}}{\chi V_t} \approx \text{const} \tag{24}$$

holds true, where λ and V_{aw} have been determined above, χ is the interplanar distance corresponding to the maximum intensity of the x-ray reflection, and V_t is the propagation rate of transverse ultrasonic waves. The last two parameters for the materials are determined from reference books [99, 100]. To elucidate the meaning of Eq. (24), data on the value of the ratio $\lambda V_{\text{aw}}/\chi V_t$ obtained for different strain modes of the investigated materials and presented in Tables 1–3 were statistically analysed in Ref. [47] for the following cases:

• linear work hardening and easy glide in single crystals and polycrystals;

• compression strain of alkali halide crystals (KCl, NaCl, and LiF);

• compression strain of rocks (marble and sandstone);

• creep of polycrystalline aluminium;

• strain caused by motion of individual dislocations in Zn, CsI, NaCl, KCl, and LiF single crystals [101, 102].

Investigations were performed for single crystals and polycrystals deformed by slipping, twinning (γ-Fe and marble), and grain boundary processes (sandstone). On diagrams $\sigma(\varepsilon)$ for the investigated materials, sections of linear strain hardening can be seen in which the phase localized plastic flow autowaves emerge. The ratios $\lambda V_{aw}/\chi V_t$ used to estimate the data are given in Tables 1–3 for 38 investigated materials. As follows from Tables 1–3, $0.2 \le \hat{Z} \le 1.1$.

To elucidate the nature of the invariant, the question about the law of $\hat{Z}$ distribution in a sample is of principal importance. To answer it, as a 0-hypothesis, it was accepted that sizes $\hat{Z}$ obey a normal law [47]. This means that the correlation of their behaviour in experimentally established limits with the behaviour of any characteristic of the material is absent.

Table 1. **A comparison of χV_t and λV_{aw} products for metals investigated [25]**

Metals	Linear work hardening stage			Easy glide stage		
	λV_{aw}, $\times 10^7$ m^2/s	χV_t, $\times 10^7$ m^2/s	$\lambda V_{aw}/\chi V_t$, $\times 10^7$ m^2/s	λV_{aw}, $\times 10^7$ m^2/s	χV_t, $\times 10^7$ m^2/s	$\lambda V_{aw}/\chi V_t$, $\times 10^7$ m^2/s
Cu	3.6	4.8	0.75	1.9	4.7	0.4
Zn	3.7	11.9	0.3	1.0	5.0	0.2
Al	7.9	7.5	1.1			
Zr	3.7	11.9	0.3			
Ti	2.5	7.9	0.3			
V	2.8	6.2	0.45			
Nb	1.8	5.3	0.33			
α-Fe	2.55	4.7	0.54	7.4	6.5	1.1
γ-Fe	2.2	6.5	0.34	2.9	6.0	0.49
Ni	2.1	6.0	0.35	1.3	6.0	0.2
Co	3.0	6.0	0.5			
Mo	1.2	7.4	0.2			
Sn	2.4	5.3	0.65	3.3	4.9	0.67
Mg	9.9	15.8	0.63			
Cd	0.9	3.5	0.2			
In	2.6	2.2	1.2			
Pb	3.2	2.0	1.6			
Ta	1.1	4.7	0.2			
Hf	1.0	4.2	0.24			

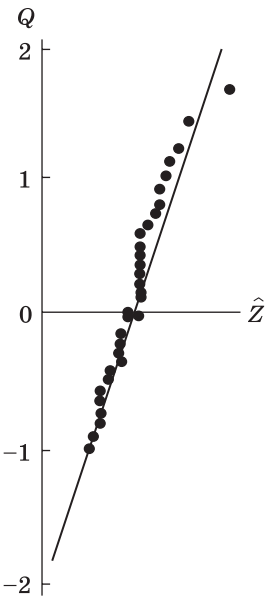

Fig. 11. To the verification of distribution type of invariant $\hat{Z}$ on the values. The correlation coefficient between Q and $\hat{Z}$ values is of about 0.98 [119]

To test the 0-hypothesis by the graphic method, data of Tables 1–3 were transformed into the variational series $\hat{Z}_1 < \hat{Z}_2 < \hat{Z}_3 < \ldots < \hat{Z}_i < \hat{Z}_{n-1} < \hat{Z}_{n=38}$ whose terms serve as arguments for the search of numerical values of quintiles $-\infty < Q < \infty$ of the normal distribution corresponding to $i(n+1)$ [47]. The hypothesis about the normal distributions of $\hat{Z}$ is accepted, if Q is actually linear in $\hat{Z}$. As can be seen from Fig. 11, the dependence $Q(\hat{Z})$ in the coordinates Q–$\hat{Z}$ is linear in character. Thus, the quantities $\hat{Z}$ obey the normal distribution, and variations of $\hat{Z}$ for $0.2 \le \hat{Z} \le 1.1$ depend only on experimental errors in measuring the parameters of the phase localized plasticity autowaves.

Thus, the average value $\langle \lambda V_{aw}/\chi V_t \rangle$, and standard error [47] were determined. It turned out that

$$\left\langle \frac{\lambda V_{aw}}{\chi V_t} \right\rangle_{n=38} = \left\langle \hat{Z} \right\rangle = 0.49 \pm 0.04 \cong \frac{1}{2}. \qquad (25)$$

Equation (25), called the *elastic–plastic strain invariant*, quantitatively relates the characteristics of the elastic waves (χ and V_t) to the characteristics of plastic flow autowaves (λ and V_{aw}), combining the elas-

Table 2. **A comparison of χV_t and λV_{aw} products for alkali-halide crystals and rocks [25]**

$\times 10^7$ m^2/s	KCl	NaCl	LiF	Marble	Sandstone
λV_{aw}	3.0	3.1	4.3	1.75	0.6
χV_t	7.0	7.5	8.8	3.7	1.5
$\lambda V_{aw}/\chi V_t$	0.43	0.4	0.5	0.5	0.4

Table 3. **A comparison of χV_t and lV_{disl} products for individual dislocation paths [25]**

$\times 10^7$ m^2/s	NaCl	LiF	CsI	KCl	Zn
lV_{disl}	4.1	4.1	1.9	4.1	1.8
χV_t	7.3	8.6	4.0	6.8	4.0
$lV_{disl}/\chi V_t$	0.56	0.47	0.47	0.6	0.45

tic ($\varepsilon_{el} \approx 1$) and plastic ($\varepsilon_{pl} \approx 1$) strain components simultaneously acting in a solid. The product χV_t describes the redistribution of elastic stresses with the velocity, V_t, and the product λV_{aw} plays the same role for the pattern redistribution with the rate V_{aw}.

Thus, the elastic–plastic strain invariant acquires the status of the parameter suitable for a description of plastic flow processes in materials irrespective of their nature and operating plasticity micromechanisms. To refine its physical meaning, we take into account that $V_t \approx \chi(\omega_D/2\pi)$ and $\hbar\omega_D \approx k_B\theta_D$, where $\hbar = h/2\pi$ is the Planck's constant, and θ_D is the Debye parameter [103]. Then

$$\lambda V_{aw} = \hat{Z}\chi V_t \approx \hat{Z}\chi^2 \frac{\omega_D}{2\pi} \approx \hat{Z}\frac{k_B}{\hbar}\left(\chi^2\theta_D\right). \qquad (26)$$

The value λV_{aw} that characterizes the plastic flow at the stage of linear work hardening can be calculated directly from Eq. (26) for the known values χ and θ_D. The results of such calculations, presented in Table 4, show that Eq. (26) correctly predicts the order of magnitude of λV_{aw}. It is well known that the Debye parameter depends on the temperature [103]. On this reason, Eq. (26) can use to predict the important temperature dependence of the plasticity parameter λV_{aw}.

5.2. Nature of the Elastic–Plastic Strain Invariant

Relating the characteristics of the elastic (χ and V_t) and plastic (λ and V_{aw}) deformation components, invariant (25), evidently, plays an important role for a description of the localized plasticity dynamics, and it is necessary to consider its nature. As shown above, the plastic strain localization is a consequence of self-organization of a nonlinear active deforming medium. As well known, the common feature of the self-or-

Table 4. **Estimations of λV_{aw} values *via* the lattice characteristics of metals [25]**

Metal	χ $\times 10^{10}$ m	θ_D K	$(\lambda V_{aw})^{(calc)}$ $\times 10^7$ m^2/s	$(\lambda V_{aw})^{(exp)}$ $\times 10^7$ m^2/s	$(\lambda V_{aw})^{(calc)}/(\lambda V_{aw})^{(exp)}$
Ni	2.03	375	1.6	2.1	0.8
Cu	2.08	315	1.4	3.6	0.4
Al	2.33	394	2.2	2.6	0.8
Mo	2.22	380	1.9	1.2	1.6
Co	2.18	385	1.9	1.3	1.5
Sn	3.75	170	2.5	2.4	1.0
α-Fe	2.02	420	1.8	2.55	0.7
In	2.72	129	0.95	2.6	0.4
Zn	2.077	234	1.0	3.7	0.3
Cd	2.34	120	0.65	0.9	0.7
Mg	2.45	318	1.9	9.9	0.2

ganization processes in an open system such as a deforming body is a decrease in the entropy in the course of processes [20]. This condition is satisfied in the process of generation of localized plastic flow autowaves [104]. On this reason, the use of the entropy to explain the invariant is well justified.

The two-component localized plasticity model is based on the emergence and destruction (relaxation) of elastic stress concentrators accompanied by generation of dislocations. This means that during deformation, the spatiotemporal distributions of the stress fields $\sigma(x, y, t)$ and plastic strains $\varepsilon(x, y, t)$ undergo interrelated transformations. The velocities V_t and V_{aw} control the transformation kinetics of the corresponding fields, and the lengths χ and λ are the spatial *scales* of these processes. For this reason, it is convenient to write invariant (25) in the form

$$\frac{\lambda V_{\text{aw}}}{\chi V_t} = \frac{\lambda/\chi}{V_t/V_{\text{aw}}} = \hat{Z} < 1, \tag{27}$$

where the ratios $\lambda/\chi = p_{\text{scale}} > 1$ and $V_t/V_{\text{aw}} = p_{\text{kin}} > 1$ make sense of the *scale* and *kinetic* thermodynamic probabilities [105]. The *scale* thermodynamic probability p_{scale} is interpreted as the number of possible nuclei of emergence of the localized plastic flow autowaves in a deforming medium, that is, it is determined by significant difference between the spatial scales of elastic and plastic deformation processes [106]. The structure parameter p_{scale} is dissipative one and causes the autowave dispersion, that is, destroys the order. As to the *kinetic* thermodynamic probability, p_{kin}, it determines the choice by a deforming system of the observable autowave rate from the range of its possible values $0 \le V_{\text{aw}} \le V_t$. This parameter, on the contrary, promotes ordering, because it can be associated with the rule of subordination of slow processes to the fast ones characteristic for synergetics [12, 15].

In this case, from Eq. (27), it follows that

$$\ln\hat{Z} = \ln p_{\text{scale}} - \ln p_{\text{kin}} \tag{28}$$

that corresponds to equations for changes in the entropy due to different scales

$$\Delta S_{\text{scale}} = k_B \ln\frac{\lambda}{\chi} = k_B \ln p_{\text{scale}}, \tag{29}$$

and different velocities

$$\Delta S_{\text{kin}} = k_B \ln\frac{V_t}{V_{\text{aw}}} = k_B \ln p_{\text{kin}}. \tag{30}$$

From Eqs. (28) to (30), we finally obtain

$$\Delta S = -k_B \ln p_{\text{kin}} + k_B \ln p_{\text{scale}} = -\Delta S_{\text{kin}} + S_{\text{scale}} = k_B \ln\frac{1}{2} < 0, \tag{31}$$

from which it follows that the entropy of the deforming system decreases during phase autowave generation. The signs of $\Delta S_{\text{scale}} > 0$ and $\Delta S_{\text{kin}} < 0$ in Eq. (31) confirm the antagonism of contributions of the scale and kinetic factors to the nature of the localized plasticity.

The parameter $\Delta S < 0$ points to the decrease in the entropy due to generation of the phase autowave of a localized flow. It is characteristic for the self-organization processes in a deforming medium. Since

$$\hat{Z} = \exp\left(\Delta S / k_B\right) \approx \frac{1}{2}, \tag{32}$$

then, $\Delta S = k_B \ln 1/2 \approx -0.7 k_B$ per elementary relaxation act.

To elucidate a nature of Eqs. (7) and (8), we consider the relationship between the elastic and plastic displacements of elements in the course of a deformation of a nearly equilibrium medium. In this case, the displacement velocities during alterations of the strain and stress fields are linear in gradients of plastic and elastic strains within the first order of smallness [105, 107], and

$$\dot{u}_{\text{pl}}^{(p)} \approx D_{\varepsilon\varepsilon} \nabla \varepsilon_{\text{pl}}, \tag{33}$$

$$\dot{u}_{\text{el}}^{(p)} \approx D_{\sigma\sigma} \nabla \varepsilon_{\text{el}}, \tag{34}$$

respectively. We also take into account the occurrence of velocities additional to Eqs. (33) and (34) due to strain–stress interactions:

$$\dot{u}_{\text{el}}^{(ad)} \approx D_{\varepsilon\sigma} \nabla \varepsilon_{\text{pl}}, \tag{35}$$

$$\dot{u}_{\text{pl}}^{(ad)} \approx D_{\sigma\varepsilon} \nabla \varepsilon_{\text{el}}. \tag{36}$$

Here, it has been accepted that $\lambda V_{aw} \equiv D_{\varepsilon\sigma}$ and $\chi V_t \equiv D_{\sigma\varepsilon}$.

Now, using Eqs. (33) to (36), one can write the equations

$$\begin{cases} \dot{u}_{\text{pl}} = D_{\varepsilon\varepsilon} \nabla \varepsilon + D_{\varepsilon\sigma} \nabla \varepsilon_{\text{el}}, & (37) \\ \dot{u}_{\text{el}} = D_{\sigma\varepsilon} \nabla \varepsilon_{\text{el}} + D_{\sigma\sigma} \nabla \varepsilon. & (38) \end{cases}$$

Their coefficients form the matrix [105]

$$\begin{bmatrix} D_{\varepsilon\varepsilon} & D_{\varepsilon\sigma} \\ D_{\sigma\varepsilon} & D_{\sigma\sigma} \end{bmatrix}$$

that explains double subscripts of the coefficients D in Eqs. (7), (8), *etc*. According to the Onsager principle [105, 107], the non-diagonal elements of this matrix are equal, that is, $\lambda V_{aw} \equiv D_{\varepsilon\sigma} \equiv D_{\sigma\varepsilon} \equiv \chi V_t$. At the same time, the diagonal elements $D_{\varepsilon\varepsilon}$ and $D_{\sigma\sigma}$, which are simultaneously the coefficients of autowave equations (7) and (8), are not necessary equal; below, it will be shown that $D_{\varepsilon\varepsilon} \ll D_{\sigma\sigma}$.

5.3. Invariant as the Master Equation of the Autowave Theory of Plasticity

Since invariant (25) relates the characteristics of simultaneously proceeding elastic and plastic processes in a deforming medium, it plays an important role of the *master equation* of autowave mechanics of localized plastic flow being developed. This is confirmed by the circumstance that invariant (25) has a number of consequences that can be used not only to understand the nature of some important features of dynamics of localized plasticity, but also to describe them quantitatively. We consider these consequences below.

5.3.1. Propagation Velocity of the Localized Plasticity Autowaves

Differentiating Eq. (25) with respect to the strain ε

$$\lambda \frac{dV_{\text{aw}}}{d\varepsilon} + V_{\text{aw}} \frac{d\lambda}{d\varepsilon} = \hat{Z}\chi \frac{dV_t}{d\varepsilon} + \hat{Z}V_t \frac{d\chi}{d\varepsilon}, \tag{39}$$

and writing the result for V_{aw}, we obtain

$$V_{\text{aw}} = \left(\frac{d\lambda}{d\varepsilon}\right)^{-1} \left(\hat{Z}\chi \frac{dV_t}{d\varepsilon} + \hat{Z}V_t \frac{d\chi}{d\varepsilon} - \lambda \frac{dV_{\text{aw}}}{d\varepsilon}\right). \tag{40}$$

The interplanar distance χ is independent on the plastic strain, so that $\hat{Z}V_t d\chi/d\varepsilon = 0$, and

$$V_{\text{aw}} = \hat{Z}\chi \frac{dV_t}{d\lambda} - \lambda \frac{dV_{\text{aw}}}{d\lambda}\ . \tag{41}$$

Transformations of Eq. (41) lead to the relationship

$$V_{\text{aw}} = \hat{Z}\chi \frac{dV_t}{d\lambda} - \chi \frac{dV_{\text{aw}}}{d\lambda}\frac{\lambda}{\chi} \approx V_0 + \frac{\Xi}{\theta}\ , \tag{42}$$

analogous to the experimentally obtained dependence $V_{\text{aw}}(\theta) \propto \theta^{-1}$, if we express the strain hardening coefficient as the ratio of the structural parameters λ and $\chi \ll \lambda$ [5], that is, as $\theta \approx \chi/\lambda$.

5.3.2. Dispersion of the Localized Plasticity Autowaves

Let us write down invariant (25) in the form

$$V_{\text{aw}} = \frac{\Theta}{\lambda} = \frac{\Theta}{2\pi} k\,, \tag{43}$$

where $\Theta = Z\chi Vt$. If $V_{\text{aw}} = d\omega/dk$, then, $d\omega = (\Theta/2\pi)kdk$. In this case,

$$\int\limits_{\omega_0}^{\omega} d\omega = \frac{\Theta}{2\pi} \int\limits_{0}^{k-k_0} k dk, \tag{44}$$

and the dispersion law for the plasticity autowaves acquires the quadratic form

$$\omega(k) = \omega_0 + \frac{\Theta}{4\pi}\left(k - k_0\right)^2, \tag{45}$$

where $\Theta/2\pi \equiv \alpha$ is the parameter used in Eq. (5).

In this case, the corresponding coefficients can also be estimated quantitatively. Writing Eq. (26) in the form

$$V_{\text{aw}} \approx \hat{Z}\chi^2 \frac{k_B\theta_D}{h}\frac{1}{\lambda} \approx \hat{Z}\chi^2 \frac{k_B\theta_D}{h} k \approx \varsigma k\ , \tag{46}$$

we can calculate the coefficient $\varsigma = \hat{Z}\chi^2 k_B\theta_D/h \approx \hat{Z}\chi^2\omega_D$ for the values $\chi^{(\text{Fe})}$, $\chi^{(\text{Al})}$, $\theta_D^{(\text{Fe})} = 420$ K, and $\theta_D^{(\text{Al})} = 394$ K [103]. Then, $\varsigma^{(\text{Fe})} \approx 3.7\cdot10^{-7}$ m^2/s and $\varsigma^{(\text{Al})} \approx 4.45\cdot10^{-7}$ m^2/s. This is in agreement with values $\varsigma^{(\text{Fe})} = (1.0 \pm \pm\ 0.08)\cdot10^{-7}$ m^2/s and $\varsigma^{(\text{Al})} = (12.9 \pm 0.15)\cdot10^{-7}$ m^2/s experimentally determined from the dependence $V_{\text{aw}}(k)$ presented in [48] and Fig. 5, *b*.

5.3.2. The Grain Size and the Localized Plasticity Autowaves

From invariant (25), it follows that

$$\lambda = \hat{Z}\chi\frac{V_t}{V_{\text{aw}}}\ . \tag{47}$$

If the velocities V_t and V_{aw} depend on the grain size δ, then, differentiation of Eq. (47) with respect to δ yields

$$\frac{d\lambda}{d\delta} = \hat{Z}\chi\frac{d}{d\delta}\left(\frac{V_t}{V_{\text{aw}}}\right) = \hat{Z}\chi\left(\frac{V_{\text{aw}}dV_t\ /\ d\delta - V_t dV_{\text{aw}}\ /\ d\delta}{V_{\text{aw}}^2}\right), \tag{48}$$

from which it follows that

$$d\lambda = \hat{Z}\chi\left(\frac{dV_t}{d\delta}\frac{1}{V_{\text{aw}}} - V_t\frac{dV_{\text{aw}}}{d\delta}\frac{1}{V_{\text{aw}}^2}\right)d\delta = \left(a_1\lambda - a_2\lambda^2\right)d\delta, \tag{49}$$

where

$$a_1 = \frac{1}{V_t}\frac{dV_t}{d\delta} = \frac{d\ln V_t}{d\delta} \quad \text{and} \quad a_2 = \frac{1}{\hat{Z}\chi V_t}\frac{dV_{\text{aw}}}{d\delta},$$

since

$$V_{\text{aw}} = \hat{Z}\chi V_t\frac{1}{\lambda}\ .$$

A solution of differential equation (49) is Verhulst function

$$\lambda(\delta) = \lambda_0 + \frac{a_1\ /\ a_2}{1 + C\exp\left(-a_1\delta\right)} \tag{50}$$

obtained experimentally for Al with grain sizes $5 \cdot 10^{-3} \le \delta \le 15$ mm. In Eq. (50), $\lambda_0 = \text{const}$, and C is the integration constant (see above).

5.3.4. Elastic–Plastic Invariant and the Hall–Petch Relationship

It is well known that the mechanical characteristics of polycrystalline materials (yield strength, flow stress, and others) depend on such structural parameter as the grain size [22, 108]. The corresponding dependences are usually linear in the 'property–$\delta^{-1/2}$' coordinates. It makes sense to check the validity of Eq. (25) for two intervals of grain sizes $5 \cdot 10^{-6} \le \delta \le 10^{-4}$ m and $10^{-4} \le \delta \le 5 \cdot 10^{-3}$ m. Results given in Table 5 indicate the validity of the elastic–plastic invariant under these conditions.

5.3.5. Scale Effect for the Localized Plasticity Autowaves

If the autowave length is measured in samples of different lengths L, then,

$$\frac{d}{dL}\left(\lambda V_{\text{aw}}\right) = \frac{d\lambda}{dL} V_{\text{aw}} + \lambda \frac{dV_{\text{aw}}}{dL} = \hat{Z} \frac{d}{dL}\left(\chi V_t\right) = 0 \tag{51}$$

and

$$\frac{d\lambda}{dL} = -\frac{\lambda}{V_{\text{aw}}} \frac{dV_{\text{aw}}}{dL}. \tag{52}$$

For $\lambda = \lambda_0 = \text{const}$ and $dV_{\text{aw}}/dL \approx V_{\text{aw}}/L$, we have $d\lambda/dL \approx (\lambda_0/V_{\text{aw}})(V_{\text{aw}}/L)$ and $d\lambda \propto dL/L$, that is, $\lambda \propto \ln L$, as established previously in Ref. [25].

5.3.6. Autowave Equation for a Plastic Flow

Let us write invariant (25) as

$$\frac{\chi}{\lambda} = \frac{V_{\text{aw}}}{V_t} \hat{Z} \tag{53}$$

and assume that $\varepsilon \approx \lambda/\chi \gg 1$ is the plastic strain. Acting with the operator $\partial/\partial t = D_{\varepsilon\varepsilon} \partial^2/\partial x^2$ on both sides of Eq. (53), we obtain

$$\frac{\partial \varepsilon}{\partial t} = \hat{Z} D_{\varepsilon\varepsilon} \left(-V_t \frac{\partial^2 V_{\text{aw}}^{-1}}{\partial x^2} + V_{\text{aw}}^{-1} \frac{\partial^2 V_t}{\partial x^2} \right) = \hat{Z} D_{\varepsilon\varepsilon} \left[-V_t \frac{\partial^2 V_{\text{aw}}^{-1}}{\partial x^2} + \frac{\partial^2 \left(V_t / V_{\text{aw}} \right)}{\partial x^2} \right]. \tag{54}$$

Table 5. **Elastic–plastic invariant for two grain-sizes' ranges [25]**

Grain size ranges, m	$\chi V_t \cdot 10^7$, m²/s	$\lambda V_{\text{aw}} \cdot 10^7$, m²/s	$\frac{\lambda V_{\text{aw}}}{\chi V_t}$	Grain size ranges, m	$\chi V_t \cdot 10^7$, m²/s	$\lambda V_{\text{aw}} \cdot 10^7$, m²/s	$\frac{\lambda V_{\text{aw}}}{\chi V_t}$
$5 \cdot 10^{-6} \le \delta \le 10^{-4}$	5.13	2.61	≈0.5	$10^{-4} \le \delta \le 5 \cdot 10^{-3}$	6.17	3.12	≈0.5

The velocity of ultrasound propagation depends weakly on the strain; so, $V_t \approx$ const in Eq. (54). Since $V_t/V_{aw} \approx \hat{Z}^{-1}\lambda/\chi \approx \varepsilon$, then,

$$\frac{\partial \varepsilon}{\partial t} = -\hat{Z}D_{\varepsilon}V_t \frac{\partial^2 V_{aw}^{-1}}{\partial x^2} + D_{\varepsilon\varepsilon}\frac{\partial^2 \varepsilon}{\partial x^2}\ . \qquad (55)$$

This relationship is equivalent to differential Eq. (7) of the reaction-diffusion type for the strain rate derived above.

5.3.7. The Taylor–Orowan Equation and Relationship to the Dislocation Theory

The main problem of the autowave approach to the plastic flow is elucidation of its relationship to the dislocation theory [4–7] traditionally used to explain the nature of work hardening in real crystals. As well known, these models are based on the Taylor–Orowan equation for dislocation kinetics [6, 7]

$$\frac{d\varepsilon}{dt} = b\rho_{md}V_{disl}\ , \qquad (56)$$

relating the plastic strain rate to the density of mobile dislocations and their rate. The comparison Eqs. (56) and (54) shows that the first term

$$-\hat{Z}D_{\varepsilon\varepsilon}V_t \frac{\partial^2 V_{aw}^{-1}}{\partial x^2}$$

in the right side of Eq. (54) is analogous to expression $b\rho_{md}V_{disl}$ in Eq. (56). Indeed, let $V_t \approx \chi\omega_D \approx b\omega_D$ and $D_{\varepsilon\varepsilon} = \hat{Z}D_{\sigma\sigma} = \hat{Z}\chi V_t$. If we set that

$$\frac{\partial^2 V_{aw}^{-1}}{\partial x^2} \approx \frac{V_{aw}^{-1}}{x^2}\ ,$$

we obtain for the dislocation chaos $x^{-2} \approx l^{-2} \approx \rho_{md}$, where l is the free path of dislocations. Then

$$-\hat{Z}D_{\varepsilon\varepsilon}V_t \frac{\partial^2 V_{aw}^{-1}}{\partial x^2} \approx -\hat{Z}^2\chi V_t^2 b\omega_D \frac{V_{aw}^{-1}}{x^2} \approx -\hat{Z}^2 bV_t \frac{V_t / V_{aw}}{l^2} \approx -\hat{Z}^2 V^{*-1} b\rho_{md}V_t\ . \qquad (57)$$

Setting $V_d \propto V_t \approx V_{disl}$, we can write $V_t \approx V_{disl}\Psi^{-1}$; so,

$$\frac{\partial \varepsilon}{\partial t} = -\frac{\hat{Z}^2}{V^*\Psi} b\rho_{md}V_{disl} + D_{\varepsilon\varepsilon}\,\partial^2\varepsilon/\partial x^2 = \alpha b\rho_{md}V_{disl} + D_{\varepsilon\varepsilon}\,\partial^2\varepsilon/\partial x^2\ . \qquad (58)$$

The relationship of autowave equations (7) with Eq. (56) of dislocation kinetics was established in Ref. [110] based on experimental data.

Equation (58) differs from the Taylor–Orowan Eq. (56) by the term $D_{\varepsilon\varepsilon}\partial^2\varepsilon/\partial x^2$ responsible for macroscopic strain redistribution over the volume, including that proceeding at a certain distance from the existing fronts. This means that the Taylor–Orowan equation is a special case of general Eq. (58) including, along with the hydrodynamic component

$f(\varepsilon) = b\rho_{md}V_{disl} \propto V_{disl}$, the diffusion-like component $D_{\varepsilon\varepsilon}\partial^2\varepsilon/\partial x^2 \propto \partial^2\varepsilon/\partial x^2$ of the strain flow.

From here, the important conclusion follows that the autowave plastic flow model is close related to the dislocation theory. It is obvious that at small dislocation densities, the application of Eq. (56) allows one to obtain correct results. However, for large strains, high defect densities, and consecutive allowance for the nonlinear dislocation properties, it must use autowave Eq. (58) [42, 111–114].

5.3.8. On the Origin of Localized Plasticity Autowaves

An analysis of the elastic–plastic invariant allows one to understand the common reason for the emergence of the localized plastic strain autowaves. According to the Taylor–Orowan Eq. (56), the condition $\dot{\varepsilon} = \text{const}$ set to a testing machine is fulfilled only for constant dislocation flow $\rho_{md}V_{disl} = \text{const}$ provided by sufficient mobile dislocation density and velocity of their motion. This condition can be violated under strain hardening, decrease in the density of mobile dislocations with increasing strain, or decrease of dislocation velocity when the effective stress decreases from σ to $\sigma - Gb\rho_{tot}^{1/2}$ [6, 7] (where ρ_{tot} is the total dislocation density). In this case, the condition $\dot{\varepsilon} = \text{const}$ can be satisfied only if the diffusion-like strain mechanism is switched by the term $D_{\varepsilon\varepsilon}\varepsilon''$ in Eq. (7) and induce the emergence of a localized plastic flow nucleus at the distance $\propto \lambda$ from the initial nucleus by one of the above-considered mechanisms. This is the reason for the formation of the localized plastic flow autowaves.

5.3.9. Spatial Scales of the Plastic Flow

The diagonal elements of the matrix of coefficients of Eqs. (37) and (38),

$$\begin{bmatrix} D_{\varepsilon\varepsilon} & D_{\varepsilon\sigma} \\ D_{\sigma\varepsilon} & D_{\sigma\sigma} \end{bmatrix},$$

can be interpreted considering that the coefficient $D_{\varepsilon\varepsilon}$ is related to the mobile dislocation density and the coefficient $D_{\sigma\sigma}$ is determined by the elastic stress distribution. Then, because of dimensionality reasons, it follows that

$$D_{\sigma\sigma} \approx \sqrt{\frac{F}{\rho_0}}, \tag{59}$$

where F is the force of sample tension during testing and

$$D_{\varepsilon\varepsilon} \approx \frac{d}{dt}\rho_{md}^{-1}. \tag{60}$$

The dislocation density ρ_{md} depends extremely on the strain [115], and its derivative with respect to time in Eq. (60) can change sign during deformation.

From Eq. (59), it follows that typically $D_{\sigma\sigma} \approx 1$ m^2/s. The value of $D_{\varepsilon\varepsilon}$ in Eq. (60) is determined less precisely, because the data on mobile dislocation density at different stages of the plastic flow available from the literature differ substantially. However, from the data [4–7], it follows that $10^{-8} \le D_{\varepsilon\varepsilon} \le 10^{-7}$ m^2/s; so, $D_{\varepsilon\varepsilon} \ll D_{\sigma\sigma}$. We note that this condition corresponding to a slower propagation of the activator (plastic strains) in comparison with the inhibitor (stresses or elastic strains) is usually for autowave generation [12–16, 34].

As already mentioned above, the coefficient $D_{\sigma\sigma}$ describes the redistribution of stresses over the volume and the coefficient $D_{\varepsilon\varepsilon}$ is determined by the reorganization of dislocation substructures. In this case, it is natural to consider that $D_{\sigma\sigma}$ and $D_{\varepsilon\varepsilon}$ characterize the macroscopic and dislocation levels of plastic flow, respectively. Taking advantage of the diffusion approach, we now express the coefficients $D_{\varepsilon\varepsilon}$ and $D_{\sigma\sigma}$ in general as the product of the scale factor $\mathcal{R}$ by the velocity $\mathcal{V}$, that is, $D = \mathcal{R}\mathcal{V}$. Here, $\mathcal{R}$ is the size of the inhomogeneity zone in the deforming system and V is the velocity of redistribution of the strain or stress. Since the coefficient $D_{\sigma\sigma}$ is associated with stress redistribution, the characteristic velocity of this process is the transverse sound velocity, V_t, that is, $\mathcal{V} = V_t \approx 10^3$ m/s. In this case, $\mathcal{R} \equiv l_\sigma = D_{\sigma\sigma}/V_t \approx 10^{-3}$ m can be identified with the scale of macroinhomogeneity of the plastic strain. For the coefficient $D_{\varepsilon\varepsilon} \approx 10^{-8}$ m^2/s, we can set $\mathcal{V} = V_{\text{disl}} \approx 10$ m/s [101]; so, in this case, $\mathcal{R} \equiv l_\varepsilon = D_{\varepsilon\varepsilon}/V_{\text{disl}} \approx 10^{-9}$ m $\approx nb$, where $n \approx 2, \ldots, 5$, that obviously corresponds to the dislocation scale of the plastic flow.

This analysis establishes the hierarchy of structural levels of plastic deformation. It implies that values of the transport coefficients $D_{\varepsilon\varepsilon}$ and $D_{\sigma\sigma}$ in Eqs. (7) and (8), characterizing the dislocation and macroscopic scales of autowave, are determined by the scales of underlying levels. Thus, the equation

$$D_{\varepsilon\varepsilon} \approx l_d V_{\text{disl}} \tag{61}$$

relates the coefficient D_ε to the dislocation free path l_ε, and the equation

$$D_{\sigma\sigma} \approx \lambda V_t \tag{62}$$

plays the same role for the macroscopic level. Results of calculations from Eqs. (61) and (62) are presented in Table 6. The coefficient $D_{\varepsilon\varepsilon}$ was estimated from the displacement of strain fronts δx during time t as $D_{\varepsilon\varepsilon} \approx (\delta x)^2/t$. The $D_{\varepsilon\varepsilon}$ values so obtained were used to calculate the scale factor $\mathcal{R}$.

We will also take into account that the presence of minimal size $l_{\min}$ that allows the implementation of such a process is characteristic for the autowaves in active media [15]. From equality of the oscillation pe-

Table 6. **The characteristics of localized plastic flow autowaves [25]**

Composition (wt.%)	$V_{aw} \cdot 10^5$, m/s	$D_{\varepsilon\varepsilon} \cdot 10^7$, m²/s	$\mathbf{R} \cdot 10^9$, m
Fe–0.1%C–2%Mn	4.5	8.1	5.3
Cu–10%Ni–6%Sn	6.5	7.6	5.2
NiTi	1.0	0.8	0.6
Ni_3Mn	10.0	13.5	6.8
γ-Fe–12%Mn	3.5	7.8	4.3
γ-Fe–0.5%N	2.7	2.0	1.0

riod $\vartheta_{os} \approx 2\pi\omega^{-1}$ and the characteristic diffusion time $\vartheta_D \approx l^2/2D$ in the system, it follows that

$$l_{\min} \approx \left(2D\vartheta_{os}\right)^{1/2} \approx \left(4\pi D/\omega\right)^{1/2}. \tag{63}$$

Using for calculation of $l_{\min}$ the characteristics of the slowest processes $D \equiv D_{\varepsilon\varepsilon} \approx 10^{-8}$ m²/s and $\omega \approx 10^{-3}$ Hz, we obtain the estimation from below $l_{\min} \approx 10^{-2}$ m, close to the observed minimal length of the sample $l_{\min}^{(exp)} \leq 2 \cdot 10^{-2}$ m, at which the autowave processes of strain localization are not observed.

5.3.10. Mobile Dislocation Density

Using Eqs. (58) and (59), from Eq. (25), we obtain

$$\frac{d}{dt}\left(\rho_{md}^{-1}\right) \approx \hat{Z}\sqrt{\frac{F}{\rho_0}} = \Omega \tag{64}$$

or

$$\frac{d}{dt}\left(\rho_{md}^{-1}\right) \approx -\rho_{md}^{-2}\frac{d\rho_{md}}{dt} = \Omega. \tag{65}$$

From here, it follows that

$$\rho_{md}^{-2} d\rho_{md} = -\Omega dt, \tag{66}$$

i.e., $\rho_{md} \propto -t^{-1}$ or $\rho_{md} \propto \varepsilon^{-1}$, since $\varepsilon \propto t$ under active loading. Gilman [115] reported this decrease of the mobile dislocation density at high strains.

5.3.11. Work Hardening Coefficient

We now take advantage of Eq. (41) for the autowave velocity and formula (45) for the dispersion obtained above to write

$$\theta = \frac{\Xi}{2\pi\alpha}\lambda = \frac{\Xi}{2\pi\hat{Z}\chi V_t}\lambda \approx \frac{\Xi}{\pi V_t}\frac{\lambda}{\chi}. \tag{67}$$

Calculation with Eq. (67) yields $\theta \approx 3 \cdot 10^{-3}$, which is close to experimental values at the stage of linear work hardening of single crystals [5–7].

5.3.12. Relationship between the Elastic and Plastic Strain Components

Discussing the physical meaning of invariant (21), we noted that to analyse relationship between the elastic, ε_{el}, and plastic, ε_{pl}, components of the total strain ε_{tot}, it is generally accepted $\varepsilon_{tot} = \varepsilon_{el} + \varepsilon_{pl} \cong \varepsilon_{pl}$, since $\varepsilon_{pl} \gg \varepsilon_{el}$. However, from Eq. (25) it obviously follows that the interrelation between the elastic and plastic components of strain is not reduced to this additive formula, but is much more complicated.

According to the developed representations, the elastic strains govern the plastic flow. In particular, the behaviour of the elastic strain field explains the formation of the macroscopic autowave scale in the course deforming media.

6. Plastic Flow as a Macroscopic Quantum Phenomenon

Measurements of the localized plasticity autowave characteristics performed for a large number of metals draw attention to a very interesting regularity. Its observation has additionally confirmed a critical importance of the elastic–plastic strain invariant given by Eq. (25) and has emphasized once again its deep physical meaning discussed in detail above.

6.1. Localized Plastic Flow and the Planck Constant

Remarkable regularity has been found by numerical analysis of the experimental data on λ and V_{aw} obtained for nineteen metals. We noticed that the products $\lambda V_{aw} \rho r_{ion}^3$ were very close to Planck's constant $h = 6.63 \cdot 10^{-34}$ J·s [116] for all investigated metals. The calculated results are presented in Table 7 together with the metal density, ρ, and ion radius, $r_{ion} \approx \chi$, borrowed from [99, 100]. The average value, calculated for nineteen metals, is $\langle h \rangle = (6.86 \pm 0.45) \cdot 10^{-34}$ J·s, and the ratio $\langle h \rangle / h = 1.3 \pm 0.06 \cong 1$.

Based on this ratio, we concluded that $\langle h \rangle = h$.

This coincidence is surprising and requires careful validation, for what the quantities $\langle h \rangle$ and h were matched using the standard statistical procedure based on the Student's paired sample t-test [47]. In calculations, the value $\langle h \rangle$ was the average of nineteen experimental measurements ($n_1 = 19$), and the value h was obtained in a single measurement ($n_2 = 1$) without variance, because it was determined with high accuracy [116]. The estimation showed that the values $\langle h \rangle$ and h are statistically identical for a 95% confidence level. Thus, for further consideration we can set that

$$\langle h \rangle = h. \tag{68}$$

Table 7. **The Planck constant, h, calculated with the use of Eq. (68) [25]**

Metal	Cu	Zn	Al	Zr	Ti	V	Nb	γ-Fe	α-Fe	Ni	Co
$h \cdot 10^{34}$	11.9	9.3	2.8	6.1	4.9	3.5	4.9	4.6	4.6	6.1	7.1

Metal	Sn	Mg	Cd	In	Pb	Ta	Mo	Hf
$h \cdot 10^{34}$	8.9	4.9	7.4	9.9	18.4	5.5	3.0	6.16

The surprising possibility of calculating the quantum constant, h, from the results of macroscopic mechanical experiments can be regarded, in general, as the obvious manifestation of the quantum character of the plastic flow in crystals. In this case, it is evident that further consideration could be based on the concept of wave-particle duality [116]. An opportunity arises to use the solids method recognized in physics [117–119], *i.e.*, to introduce a specific quasi-particle associated with the localized plastic flow autowave. This gives us a clue to the most distinctive features of the plastic flow and thus provides additional insight into the plasticity problems. By this reason, the next step in the development of this model is a quantum representation of the plastic flow. This necessitates the introduction of the quasi-particle corresponding to the localized plastic flow autowave. This idea will provide a better insight into the nature of plasticity. We call such hypothetic quasi-particle the *autolocalizon* [120, 121].

6.2. Introduction of a Quasi-Particle Related to the Plasticity

To develop this point of view, it is necessary to find the principal characteristics of the autolocalizon as a quasi-particle related to the localized plastic flow autowave. For this aim, it is convenient to use the traditional for quantum mechanics considerations onto the problem of *wave–quasi-particle duality* [103, 116, 117].

Clearly, the characteristics of the quasi-particle have to be related to those of the autowave. The effective mass of the autolocalizon is of principal importance. By definition [116],

$$m_{\text{ef}}^{(1)} = \hbar \frac{\partial^2}{\partial k^2} \left[\omega(k) \right]. \tag{69}$$

Equation (69) describes the first method of calculating the effective masses for Al and γ-Fe, for which data are available on the dispersion relationship $\omega(k)$. The second method was proposed in Refs. [118, 119]. Using the de Broglie formula [116], the effective mass can be expressed in terms of the velocity of localized plastic flow autowave as

$$m_{\text{ef}}^{(2)} = \frac{h}{\lambda V_{\text{aw}}}. \tag{70}$$

Finally, using Eq. (68)

$$m_{\text{ef}}^{(3)} = \rho r_{\text{ion}}^3 , \tag{71}$$

we obtain the third method of quantitative estimation of the effective mass.

Calculations with the help of Eqs. (69)–(71) were carried out for all investigated metals. As found, $\langle m_{\text{ef}}^{(1)} \rangle \approx \langle m_{\text{ef}}^{(2)} \rangle \approx \langle m_{\text{ef}}^{(3)} \rangle \approx 1.8 \pm 0.3$ a.m.u. (atomic mass units). This suggests that the value $\langle m_{\text{ef}} \rangle = 1.8 \pm 0.3 \approx 2.0$ a.m.u. can be accepted as the rough estimate of the effective autolocalizon mass, *i.e.*, $m_{a-1} \equiv \langle m_{\text{ef}} \rangle \approx 2.0$ a.m.u.

The problem exists to understand how the effective mass arises. To solve it, we took into account that the dislocation mobility under plastic deformation depends on the viscosity B of phonon and electron gases in solids [119, 121]. If the dislocations travel uniformly, *i.e.*, $V_{\text{disl}} = \text{const}$ and $\dot{V}_{\text{disl}} = 0$, the viscous drag force per unit length is $F_{\text{vis}} \propto BV_{\text{disl}} \propto V_{\text{disl}}$ [63]. However, the inertial drag force $F_{\text{vis}} \propto \dot{V}_{\text{disl}}$ [62] appears in addition to the viscous drag force F_{vis} during an accelerated motion of dislocation when $V_{\text{disl}} \neq \text{const}$ and $\dot{V}_{\text{disl}} \neq 0$. Evidentially, the second variant is more realistic for the dislocation behaviour in the localized plasticity autowaves. Then, the total drag force is

$$F_{\Sigma} = F_{\text{vis}} + F_{\text{in}} \approx BV_{\text{disl}} + \frac{B}{\nu}\dot{V}_{\text{disl}} = B\left(V_{\text{disl}} + \frac{\dot{V}_{\text{disl}}}{\nu} \right). \tag{72}$$

Here ν is the frequency of relaxation acts, and the ratio B/ν can be interpreted as the total virtual effective mass per dislocation length unit (the effective mass). Thus, the additional drag force of inertial origin $F_{\text{in}} \approx (B/\nu)\dot{V}_{\text{disl}} \propto \dot{V}_{\text{disl}}$ appears in Eq. (72). Since the contributions of phonon and electron gases to the dislocation drag coefficient are additive, *i.e.*, $B = B_{\text{ph}} + B_{\text{e}}$ [63], it follows from Eq. (72) that

$$F_{\Sigma} \approx B_{\text{ph}}V_{\text{disl}} + B_{\text{e}}V_{\text{disl}} + \frac{B_{\text{ph}}}{\nu}\dot{V}_{\text{disl}} + \frac{B_{\text{e}}}{\nu}\dot{V}_{\text{disl}} . \tag{73}$$

In Eq. (73) the coefficients of the dislocation acceleration $\dot{V}_{\text{disl}}$ make sense of the virtual mass, including contributions from both phonon, B_{ph}/ν, and electron, B_{e}/ν, gas viscosities, correspondingly. Then, we have for the inertial term

$$F_{\text{in}} \approx \frac{B_{\text{ph}}}{\nu}\dot{V}_{\text{disl}} + \frac{B_{\text{e}}}{\nu}\dot{V}_{\text{disl}} \approx \frac{B_{\text{ph}} + B_{\text{e}}}{\nu}\dot{V}_{\text{disl}} . \tag{74}$$

As demonstrated below, the term with the electron gas viscosity, B_{e}/ν, can give rise to an interesting additional effect. Following [117], we consider here that the velocities of the autowave and autolocalizon that corresponds to it are equal, *i.e.*, $V_{a-1} = V_{\text{aw}}$. Another autolocalizon characteristic can be calculated using the standard representation [117]. The main characteristics of the hypothetic autolocalizon are presented in

Table 8. These considerations elucidate the origin and the physical sense of the autolocalizon.

Now let us consider some possibilities offered by this approach. Bearing in mind Eq. (70), we can rewrite the elastic–plastic strain invariant (25) in the form

$$\frac{h}{\lambda V_{\text{aw}}} \approx \hat{Z}^{-1} \frac{h}{\chi V_t}, \tag{75}$$

where $h/\chi V_t = m_{\text{ph}}$ and $h/\chi V_{\text{aw}} = m_{a-1}$ are the phonon and autolocalizon masses, respectively. In this case, from Eq. (75), it follows that $m_{a-1} \approx \approx m_{\text{ph}} \approx \hat{Z}^{-1} 2 m_{\text{ph}}$. Hence, Eq. (75) accounts for the mechanism proposed in Ref. [122] to explain dislocation generation in the lattice due to the phonon condensation.

Recall that the ideas about the role of quasi-particles in plasticity physics have long been in the air. The proposed concept was elaborated within the conventional approach adopted in solid-state physics that involves the introduction of a quasi-particle for a description of the wave processes. By way of example, it is just suffice to mention the elementary excitations in media [117].

Thus, the authors of Ref. [123] made one of the first attempts of this kind. They introduced a quasi-particle called *crackon* to address self-similar mechanisms of brittle crack propagation. Steverding [124] made use of quantization of elastic waves propagating in solids at fracture. Zhurkov [125] introduced the elementary excitation in crystals under deformation, which he called *dilaton*. The author of Ref. [81] proposed the possible existence of a specific deformation or fracture precursor. He coined the name *frustron* for this phenomenon.

Generally, all above-enumerated examples seem explained as the attempts to introduce the quantum mechanics principles into plasticity physics. This idea looks promising because it spreads the rules and the apparatus of this science on plasticity physics. Thus, for example, authors of [126, 127] used the quantum tunnelling mechanism to explain the low-temperature features of processes involving dislocation breaking from local obstacles. Later on, authors of [128] supplied inexact explanation of this phenomenon for the case of dislocation motion in the Peierls relief. Without doubt, ideas of this kind are transparent

Table 8. **The principal characteristics of the autolocalizon [25]**

Characteristic	Formulae	Value
Dispersion law	$\omega(k) \propto 1 + k^2$	—
Mass	$m_{a-1} = m_{\text{ef}} \equiv h/\lambda V_{\text{aw}}$	1.8 ± 0.3 a.m.u.
Rate	$V_{a-1} \equiv V_{\text{aw}}$	$10^{-5} - 10^{-4}$ m·s^{-1}
Momentum	$p = \hbar k \equiv h/\lambda$	$(6-7)\cdot 10^{-32}$ J·s·m^{-1}

enough; the underlying theoretical premises are based on the space quantization related to the discreteness of the crystal lattice in which generation and evolution of elementary plasticity events and fracture take place.

The autowaves and the quasi-particle concepts are complementary and interrelated by the general physical principles. Indeed, the above-described idea allows one to simplify significantly a solution of some problems of autowave plasticity. Thus, one can estimate the length of the localized plastic flow autowave in this framework. With this aim in view, the motion of autolocalizon is considered in the phonon gas. In view of fluctuations of the phonon gas density, it is proposed that the autolocalizon moves similar to the Brownian particle. In accordance with Einstein's theory [66, 105, 129], the free path of the Brownian particle is

$$S \approx \sqrt{\frac{k_B T}{\pi B r_{\text{a-1}}}}\,\tau\,, \tag{76}$$

where B is the dynamic viscosity of the phonon gas and the characteristic time is estimated as $\tau \approx 2\pi/\omega_{\text{aw}} \approx 10^3$ s (ω_{aw} is the frequency of the plastic flow autowave).

Hence, the free path of the quasi-particle is represented as a correlation radius of localized plasticity zones (autowave length λ). Assume that the autolocalizon has the size $r_{a-1} \approx 10^{-10}$ m, $\tau \approx 10^3$ s, $B \approx 10^{-4}$ Pa·s [63], and T = 300 K. The resultant value is $S \approx 10^{-2}$ m, which is evidently close to the experimentally obtained autowave length, *i.e.*, $S \approx \lambda$. This coincidence is the good evidence in favour of the *autowave–autolocalizon duality* for description of the plasticity phenomenon.

Thus, it can be concluded that the application of Eq. (76) yields equivalent numerical estimates of the autowave length. This suggests that both the autowave and the quasi-particle concepts correspond to the duality principle. The proposed representation appears to be productive for theoretical purposes, in particular, for plasticity physics, because various estimates could be simplified with its help.

6.3. Plasticity in the Line of Other Macroscale Quantum Phenomena

The obvious evidences in favour of the quantum character of plasticity, obtained above, are required to define more precisely the characteristics of autolocalizons. In addition, it is necessary to compare the plasticity phenomena with other quantum regularities observable on the macroscopic level.

A close connection has been established earlier in Refs. [25, 41, 60] between the deformation and the acoustic characteristics of the deformable medium. This suggests that the deformation processes can be described by a hybridized excitation spectrum shown in Fig. 12. This

spectrum was obtained by the imposition of two dependences: the linear dispersion relation $\omega \approx V_t k$ for acoustic waves (phonons) [96] and the quadratic dispersion relation $\omega = \omega_0 + \alpha(k - k_0)^2$ experimentally established for localized plasticity autowaves or autolocalizons in [48].

To validate the hybridized dependence $\omega(k)$, the coordinates $\hat{\omega}$ and $\hat{\lambda}$ were estimated for the point of intersection of the plots in the high-frequency spectral range. The frequency $\hat{\omega} \approx \omega_D$ and wave number $\hat{k}$ correspond to the minimal elastic wavelength, which is of the order of the distance between closely packed planes, *i.e.*, $\hat{k} \approx 2\pi/\chi$. This evidence indicates that the generalized dispersion relation holds true for both phonons and autolocalizons.

The dispersion curve in Fig. 12 shows a remarkable analogy with the dispersion relation obtained for ^{4}He superfluid [107]. The latter dispersion relation shows a minimum corresponding to the origination of *rotons*, *i.e.*, bosons introduced by Landau to explain the superfluidity nature and having the effective mass $m_{\text{rot}} \approx 0.64$ a.m.u. [107]. Moreover, the quadratic dispersion law obtained for the rotons is similar to the autowave dispersion described by Eq. (5). This is indicative of a possible similarity between the localized plasticity and the superfluidity. It remains to be seen whether this is a formal similarity or it has a physical sense.

Additional argument in favour of these attractive conjectures is based on an analogy. The ^{4}He superfluidity is attributed to the occurrence of normal and superfluid components in ^{4}He liquid at the temperature $T \leq 2.17$ K; the corresponding dynamic viscosities obtained for these components are $\hat{\eta}_{\text{sf}} \to 0$ and $\hat{\eta}_n \gg \hat{\eta}_{\text{sf}}$. Analogously, the plastic flow in the deformable medium would involve both the motion of individual material volumes engendered by changing and the high-velocity dislocation motion. There is the following argument in favour of this point of view. Slow processes correspond to high viscosity of the material, $\hat{\eta}_{\text{mat}} = G\tau \approx 5 \cdot 10^{12}$ Pa·s (here, $G \approx 5 \cdot 10^{10}$ Pa is the shear modulus, and $\tau = \omega_{\text{aw}}^{-1} \approx 10^2$ s is the period of the autowave). The rate of fast dislocation motion, $V_{\text{disl}} \approx (b/B)\sigma$, is controlled, as discussed above, by the viscosity of the phonon and electron gases, $B = B_{\text{ph}} + B_{\text{e}} \approx 10^{-4}$ Pa·s [63].

It is important to note that $\hat{\eta}_{\text{mat}}/B \approx 10^{16}$. It is attractive to use here the Dirac *Large Number Hypothesis* [130], according to which similar dimensionless ratios do not appear randomly and must be related to analogous ratios of other characteristics. It is easy to find that $\hat{\eta}_{\text{mat}}/B \approx \approx \omega_D/\omega_{\text{aw}} \approx (\lambda/\chi)^2 \approx 10^{16}$, and we can write

$$\frac{\lambda^2/\chi^2}{\omega_D/\omega_{\text{aw}}} \approx \frac{\lambda^2\omega_{\text{aw}}}{\chi^2\omega_D} \approx \frac{\lambda V_{\text{aw}}}{\chi V_t} \approx 1, \tag{77}$$

where we have designated $\lambda\omega_{\text{aw}} = V_{\text{aw}}$ and $\chi\omega_D = V_t$. Apparently, this can be independently derived based on the elastic–plastic strain invariant.

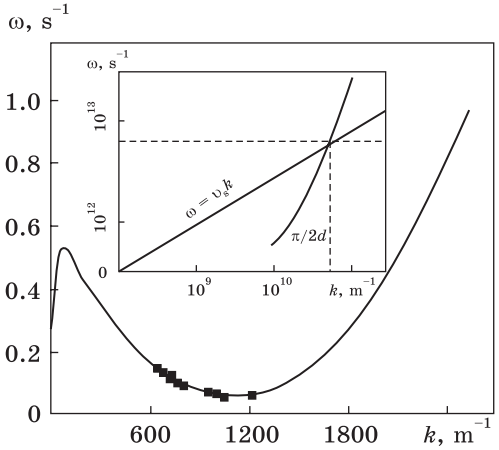

Fig. 12. Generalized dispersion curve for plastic deforming medium. The inset shows the high-frequency branch of the dispersion relation [119]

Three macroscopic quantum effects are well known in physics: superconductivity, superfluidity [107], and the quantum Hall effect [131]. The characteristics of these effects are presented in Table 9. Based on the data obtained in this work, the localized plasticity phenomenon might be included in the same list. In what follows, we try to apply the quasi-particle approach to an analysis of the Portevin–Le Chatelier effect of serrated plastic deformation [31, 57]. Assume that autowaves having length λ are arranged along the sample length L. Then the number of autowaves is given as $\lambda = L/m$, where $m = 1, 2, 3, \ldots$. The deformed sample has the length $L \approx \approx L_0 + \delta L$ (here, L_0 is initial sample length); hence, $\delta L \approx \lambda$. Thus, from Eq. (70), it follows that

$$\delta L \approx \frac{h}{\rho_0 \chi^3 V_{\text{aw}}} m \approx \frac{h}{m_{\text{a-l}} V_{\text{aw}}} m \,. \tag{78}$$

The autolocalizon mass m_{a-1} appears in Eq. (78), which confirms that a jump-wise elongation of the tensile sample is proportional to m, *i.e.*, $\delta L \propto m$. For the linear work hardening stage, $V_{\text{aw}} = \text{const}$; hence, $h(\rho_0 \chi^3 V_{\text{aw}})^{-1} = \text{const}$ for each element. Given sufficient instrumentation sensitivity, the recorded curves $\sigma(\varepsilon)$ will exhibit a jump-like behaviour; moreover, accommodation of the sample length will occur to fit the general autowave pattern. Depending on the kind of the material, the deformation occurs via different mechanisms. Numerical estimates show that, for $m = 1$, $\rho_0 \approx 5 \cdot 10^3$ kg/m^3 and $\chi \approx 3 \cdot 10^{-10}$ m the elongation jump is $\delta L_{m=1} \approx 10^{-4}$ m. For the length of the sample $L \approx 10^{-1}$ m, the elongation jump corresponds to the deformation jump $\delta \varepsilon_{m=1} \approx 10^{-3}$, which is close to the experimentally obtained value [31].

Moreover, it also follows from Eq. (78) that an increase in the loading rate would cause a decrease in the deformation jumps, *i.e.*, $\delta L \propto V_{\text{aw}}^{-1}$. This inference is supported by the experimental results obtained for Al samples tested at 1.4 K and different loading rates in [50]. Thus, the autowave rate was found to be proportional to the motion rate of the testing machine crossheads, *i.e.*, $V_{\text{aw}} \propto V_{\text{mach}}$. According to Eq. (74), the

velocity V_{aw} will increase with rate V_{mach}, while the deformation jump magnitude will grow less.

7. Autowave Plasticity and Periodical Table of Elements

The problem of physical description of the plasticity nature has been relevant to date. For progress in this area, information is important on the dependences of the metal plasticity on their positions in the (Mendeleev's) Periodic table of the elements, analogous to the well-known dependences of their physical properties on atomic numbers [132].

7.1. Investigated Metals and Experimental Results

The investigations of localized plastic flow was performed for nineteen metals from the 3rd, 4th, 5th, and 6th periods of the Periodic table of the elements, as shown in Table 10. At the bottom of it, the numbers of conduction electrons, n, per unit cell [133] are given. This quantity is proportional to the electron gas density. It is well known that the position of elements in the Periodic table is determined by the electronic structure of their atoms. In this case, the serial number N of the period coincides with the number of electronic shells of the corresponding atoms, and the number of conduction electrons per unit cell, n, for all investigated metals, except transition metals, Fe, Co, and Ni, coincides with the serial number of the group in the Periodic table [132].

Our analysis of the data obtained demonstrated that at least within interval $12_{(Mg)} \le Z \le 82_{(Pb)}$ (here, Z is the atomic number of the element) the plasticity parameter λV_{aw} markedly oscillates about its average value. According to the data [134–136], these oscillations correspond to the behaviour with increasing Z of some independently determined characteristics of the lattice, for example, of the Debye temperature, binding energy, density, melting temperature, elastic modulus, electron work function, and so on [134]. Such correspondence is illustrated by

Table 9. **A comparison of the macroscopic quantum effects, where e denotes an electron charge, c is a speed of light, r is the vortex radii in superfluidity ^{4}He**

Phenomenon	Characteristic	
	Value	Formulae
Superconductivity [117]	Magnetic flux	$\Phi = (\pi\hbar c/e)m$
Superfluidity [117]	Rotational velocity of vortexes in superfluid ^{4}He	$\upsilon = (\hbar/A_{He})(1/r)m$
Quantum Hall effect[130]	Hall resistance	$R_H = (h/e^2)(1/m)$
Serrated strain by the Portevin–Le Chatelier effect	Elongation jump magnitude	$\delta L = mh/(\rho r_{ion}^3 V_{aw})$

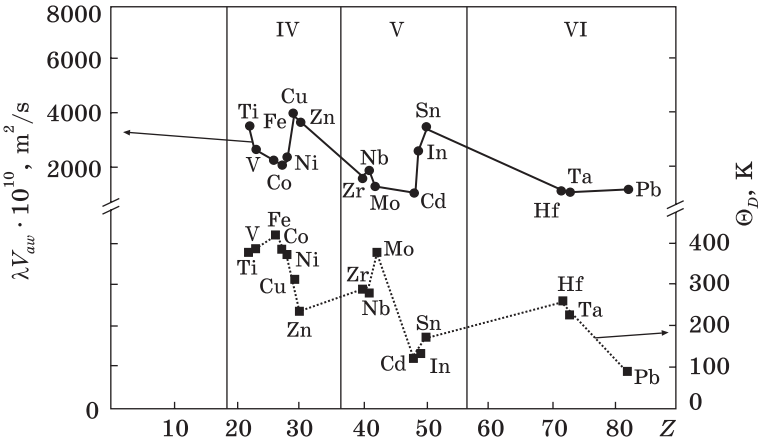

Fig. 13. The oscillations of the plasticity parameter of metals (upper curve) and of the characteristic Debye's parameter (lower curve) as a functions of atomic number of elements, Z [121]

the periodic matched behaviour of the dependences of λV_{aw} and of the characteristic Debye's parameter on the atomic number Z shown in Fig. 13.

As follows from Table 10, experimental values of the invariant $\langle \hat{Z} \rangle_i$ for the 3rd–6th periods of the Periodic table of the elements somewhat differ from each other. To test the significance of this difference, we used the statistical procedure to compare the average values of the invariants $\langle \hat{Z} \rangle_i$ for these periods according to the Student paired t-test [47].

Calculations of the t-criteria for pairs of values of the elastic–plastic invariant being compared showed that the difference in values $\langle \hat{Z} \rangle_3$,

Table 10. **Positions of the investigated metals in the Periodic table**

Periods	Series	Metals Groups of the Periodic table									$\frac{\lambda V_{aw}}{\chi V_t} = Z$
		I	II	III	IV	V	VI	VIII			
3	III		$_{12}$Mg	$_{13}$Al							$\langle \hat{Z} \rangle_3 = 0.57 \pm 0.63$
4	IV				$_{22}$Ti	$_{23}$V		$_{26}$Fe	$_{27}$Co	$_{28}$Ni	$\langle \hat{Z} \rangle_4 = 0.50 \pm 0.15$
	V	$_{29}$Cu	$_{30}$Zn								
5	VI				$_{40}$Zr	$_{41}$Nb	$_{42}$Mo				$\langle \hat{Z} \rangle_5 = 0.48 \pm 0.15$
	VII		$_{48}$Cd	$_{49}$In	$_{50}$Sn						
6	VIII				$_{72}$Hf	$_{73}$Ta					$\langle \hat{Z} \rangle_6 = 0.69 \pm 0.45$
	IX				$_{82}$Pb						
n		1	2	3	4	5	6	8	9	10	[133]

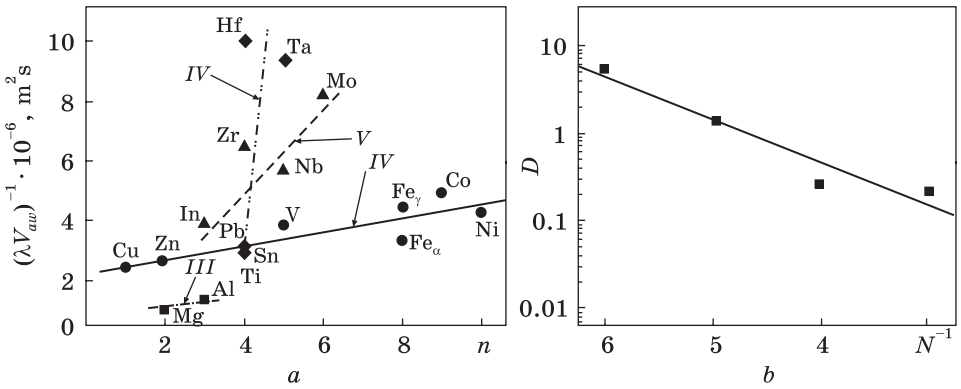

Fig. 14. The dependence of $(\lambda V_{aw})^{-1}$ on the number of electrons per unit cell n (*a*); the coefficient D in Eq. (79) as a function of the period number N (*b*) [25]

$\langle\hat{Z}\rangle_4$, $\langle\hat{Z}\rangle_5$, and $\langle\hat{Z}\rangle_6$ was statistically insignificant, so that with a probability of ≈0.85, these values belonged to one general population. Averaging over all nineteen metals yielded $\langle\hat{Z}\rangle_{5Me} \approx 1/2$. This estimate coincides with the value reported earlier in Ref. [25] for metals and non-metallic materials.

This suggests that the value of invariant (25) is independent of the serial number of the period in which the investigated metal is put in the Periodic table. In other words, the possibility has been confirmed to consider relation (1) as the universal invariant characteristic of the development of the localized plastic yield at the stage of linear work hardening.

As to the plasticity parameter λV_{aw}, it correlates with a number of other physical properties, as shown in Fig. 14, *a*. In this case, however, the corresponding dependences are split according to the serial numbers of the periods, to which the investigated metals belong.

An analysis of the behaviour of the parameter λV_{aw} within each period of the Periodic table of the elements demonstrated, in particular, that the value $(\lambda V_{aw})^{-1}$ is proportional to the number n of the conduction electrons per unit cell of the metal [133]. The existence of this relationship was already indicated in the works [118, 119], but, only after investigation of the sufficient number of metals, it became possible to highlight the separation over the periods of the Table of the elements.

It turned out that inside each investigated period, the linear dependence

$$(\lambda V_{aw})^{-1} \approx C + Dn \tag{79}$$

was observed, where the coefficients C and D differ for the elements of the 3rd–6th periods. Experimental data processing demonstrated that the coefficient D in Eq. (79) is given by the formula (Fig. 14, *b*)

$$D \approx D_0 \exp(-q/N), \tag{80}$$

where N = 3, 4, 5, and 6 is the serial number of the period in the Peri-

odic table of the elements, and D_0 and q are constants. The correlation coefficient between $\ln D$ and N^{-1} was close to (−1).

Thus, it was established that during deformation of a solid, the plastic yield localization parameters (the autowave characteristics of the process) were related with the characteristics of the electron structure of metals, that is, with the position the metal occupied in the Periodic table of the elements. This relationship was manifested through the complicated dependence of the macroscopic characteristic of the evolution of the autowave localized plasticity, λV_{aw}, simultaneously on the serial numbers of groups n and periods N of the Periodic table of the elements.

7.2. On the Nature of the Regularities Above

Understanding of the results presented above is aimed at a comparison of values of the elastic–plastic strain invariant given by Eq. (25) for different periods the Periodic table of elements (Table 10). It is important for the elucidation of the nature of the dependence of the autowave plasticity parameter λV_{aw} on the electron density for all the investigated metals, *i.e.*, on the position of elements in the Periodic table.

From Fig. 14, *a* and Eq. (79), it follows that $(\lambda V_{aw})^{-1} \propto n$ for metals of the 3rd–6th periods. When analysing the meaning of this dependence, primary attention should be paid to the fact that we can easily go from the parameter $(\lambda V_{aw})^{-1}$ to the de Broglie equation for the effective mass $m_{ef} = h/\lambda V_{aw}$. The data shown in Fig. 14, *a* demonstrate that $m_{ef} \propto n$. Apparently, this dependence is very important and must be explained. It is possible to use for these aims the considerations about the nature of the autolocalizon (see above).

As follows from Eq. (74), effective virtual mass, m_{ef}, depends on the viscosity of phonon and electron gases in crystals [63]. In this circumstance, the expression for the drag force, acting on dislocation (73), incorporates the term $(B_e/\nu)\dot{V}_{disl}$, described the electron gas contribution in this force. It is well known that the electron viscosity coefficient, B_e, is proportional to electron gas density, which is characterized by the number n in Table 10 [101]. Thus, Fig. 14, *a* corresponds to the dependence $(\lambda V_{aw})^{-1} \propto m_{ef} \propto B_e \propto n$.

For the metals of the 4th and 5th periods, it was found that

$$\left(\lambda V_{aw}\right)^{-1} \propto \exp\left(\frac{\chi}{\chi^*}\right). \qquad (81)$$

It is equivalent, evidentially, to $\ln(\lambda V_{aw})^{-1} \propto \chi$ (Fig. 15), and besides the correlation coefficients between the values $\ln(\lambda V_{aw})^{-1}$ and χ are $\xi_4 = -0.53$ and $\xi_5 = -0.89$, respectively. As to the quantity χ^*, it is close to the interplanar distance corresponding to the maximal intensities of x-ray

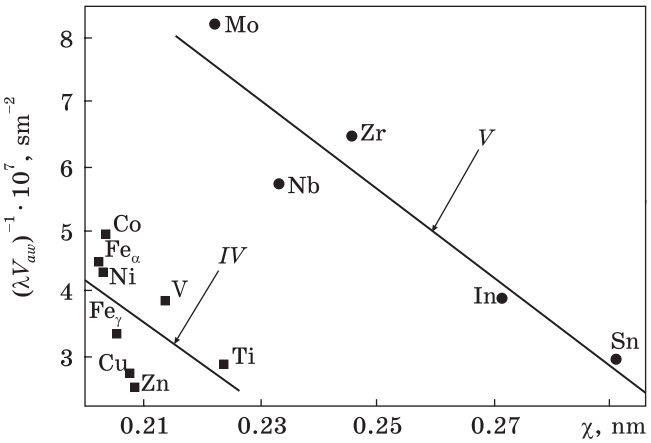

Fig. 15. The correlation between value $(\lambda V_{aw})^{-1}$ and the interplanar distance for 4-th and 5-th periods of the Periodic table of the elements [120]

reflection for K and Rb, from which the 4th and 5th periods begin. So, for the 4th period, $3.64 \cdot 10^{-10} = \chi_4^* \approx \chi_K = 3.75 \cdot 10^{-10}$ m, and for the 5th period, $4.52 \cdot 10^{-10} = \chi_5^* \approx \chi_{Rb} = 4.33 \cdot 10^{-10}$ m [99]. This correlation can provide a basis for predicting patterns of plastic flow of metals based on their lattice characteristics.

The results obtained demonstrate that during plastic flow in metals, the elastic–plastic strain invariant $\hat{Z}$ is independent of the element position in the Periodic table, whereas the plasticity characteristics (λV_{aw}) or $(\lambda V_{aw})^{-1}$ at the linear work hardening stage correlate with the characteristics of the electron structure of metals. This correlation is manifested through the change of the macroscopic characteristics of localized plasticity autowave propagation at the stage of linear work hardening depending on the number of valence electrons. This dependence is explained by the electron gas contribution into dislocation drag. These data indicate directly that the nature of the electron gas contribution to the force of drag is more complex in character than that foreseen by traditional theories [137–139].

8. Conclusion

The new approach based on the synergetics is suggested for the explanation of plastic flow regularities. Similar representations developed for a description of physical nature of plastic strain in solids consider the activity, nonlinearity, and nonequilibrium of a deforming medium as well as irreversibility of the deformation in it. These representations put at the forefront the macroscopic autowave features of plastic flow dynamics. A deforming sample in tension at a constant velocity behaves as a universal generator of autowave modes. Within the limits of this approach, the localized plastic flow is described by the two-component model based on causal relationship between elementary plasticity events

and signals of acoustic emission they generated. The model can be used to estimate the spatial and time parameters of the deformation process.

The natural relationship has successfully been found between the developed autowave theory of plastic deformation and the dislocation theory. It turned out that the latter is the limiting case of the former for small dislocation density. This makes it possible to use the existing dislocation models to explain the mechanisms that control the formation of the localized plasticity autowaves.

The suggested interpretation of the effective mass m_{ef} emphasizes the direct relationship of the macroscopic localized plastic strain characteristics λ and V_{aw} with the parameter of the electronic structure of metal — the number of electrons per unit cell. The above-considered mechanism based on the existence of mechanical relationship between the moving dislocations and the electronic gas is indirectly confirmed by investigations performed in Ref. [140] that related the electric potential on the surface of a deforming metal sample with entrainment of conduction electrons by moving dislocations during jump-like plastic deformation.

Thus, it has been established that the plasticity of metals is largely determined by their position in the Periodic table of the elements. Results of the quantitative experimental research of the complex characteristics of the development of localized plastic strain for 19 metals belonging to the 3^{rd}–6^{th} periods of the Periodic table have shown that the value of the elastic–plastic strain invariant is independent of the position of the element in the Periodic table and can be considered as the universal characteristic of plastic yielding.

Acknowledgment. The work was performed according to the Government research assignment for Institute of Strength Physics and Materials Science of Siberian Branch of the Russian Academy of Sciences (project FWRW-2021-0011).

REFERENCES

1. F. Hund, *Geschichte der Quanten Theorie* (Zürich: Bibl. Inst.: 1975) (in German).
2. R. Asaro and V. Lubarda, *Mechanics of Solids and Materials* (Cambridge: University Press: 2006).
3. E.C. Aifantis, *Acta Mech.*, **225**: 999 (2014); https://doi.org/10.1007/s00707-013-1076-y
4. D. Kuhlmann-Wilsdorf, *Dislocations in Solids* (Eds. F.R.N. Nabarro and M.S. Duesbery) (Amsterdam: Elsevier: 2002).
5. A. Argon, *Strengthening Mechanisms in Crystal Plasticity* (Oxford: University Press: 2008); https://doi.org/10.1093/acprof:oso/9780198516002.001.0001
6. D. Hull and D.J. Bacon, *Materials Today*, **14**, No. 10: 502 (2011); https://doi.org/10.1016/S1369-7021(11)70217-6

7. U. Messerschmidt, *Dislocation Dynamics during Plastic Deformation* (Berlin: Springer: 2010); https://doi.org/10.1007/978-3-642-03177-9
8. R. Abu Al-Rub and G.Z. Voyiadjis, *Int. J. Plast.*, **22**, No. 4: 654 (2006); https://doi.org/10.1016/j.ijplas.2005.04.010
9. L.S. Langer, E. Bouchbinder, and T. Lookman, *Acta Mater.*, **58**, No. 10: 3718 (2010); https://doi.org/10.1016/j.actamat.2010.03.009
10. H.M. Zbib and T.D. de la Rubia, *Int. J. Plast.*, **18**, No. 9: 1133 (2002); https://doi.org/10.1016/S0749-6419(01)00044-4
11. A. Seeger and W. Franck, *Non-Linear Phenomena in Material Science* (Eds. L.P. Kubin and G. Martin) (New York: Trans. Tech. Publ.: 1987).
12. G. Nicolis and I. Prigogine, *Self-Organization in Nonequilibrium Systems. From Dissipative Structures to Order through Fluctuations* (New York: John Wiley and Sons: 1977).
13. G. Nicolis and I. Prigogine, *Exploring Complexity. An Introduction* (New York: W.H. Freeman and Company: 1989).
14. A. Olemskoi and A. Savelyev, *Phys. Rep.*, **419**, Nos. 4–5: 145 (2005); https://doi.org/10.1016/j.physrep.2005.08.003
15. H. Haken, *Information and Self-Organization. A Macroscopic Approach to Complex Systems* (Berlin: Springer: 2006).
16. V.I. Krinsky, *Self-Organization: Autowaves and Structures Far from Equilibrium* (Berlin: Springer-Verlag: 1984).
17. W. Ebeling, A. Engeland, and R. Feistel, *Physik der Evolutionprocesse* (Berlin: Akademie Verlag: 1992) (in German).
18. H.J. Jensen, *Self-Organized Criticality. Emergent Complex Behavior in Physical and Biological Systems* (Cambridge: University Press: 1998).
19. S.P. Kurdyumov, *Int. J. Mod. Phys. C*, **1**, No. 4: 299 (1990); https://doi.org/10.1142/S0129183190000177
20. Y.L. Klimontovich, *Zs. Phys. B*, **66**: 125 (1987); https://doi.org/10.1007/BF01312769
21. A. Scott, *Nonlinear Science. Emergence and Dynamics of Coherent Structures* (Oxford: University Press: 2003).
22. J. Pelleg, *Mechanical Properties of Materials* (Dordrecht: Springer: 2013); https://doi.org/10.1007/978-94-007-4342-7
23. L.B. Zuev, V.I. Danilov, N.V. Kartashova, and S.A. Barannikova, *Mater. Sci. Eng. A*, **234–236**: 699 (1997); https://doi.org/10.1016/S0921-5093(97)00242-6
24. P.K. Rastogi, *Digital Speckle Interferometry and Related Techniques* (Ed. P.K. Rastogi) (New York: John Wiley and Sons: 2001).
25. L.B. Zuev, *Autowave Plasticity. Localization and Collective Modes* (Moscow: Fizmatlit: 2018) (in Russian).
26. A. Asharia, A. Beaudoin, and R. Miller, *Mat. Mech. Solids*, **13**: 292 (2008); https://doi.org/10.1177/1081286507086903
27. R.J. McDonald, C. Efstathiou, and P. Kurath, *J. Eng. Mat. Tech.*, **131**: 652 (2009); https://doi.org/10.1115/1.3120410
28. C. Fressengeas, A. Beaudoin, D. Entemeyer, T. Lebedkina, M. Lebyodkin, and V. Taupin, *Phys. Rev. B*, **79**, No. 1: 14108 (2009); https://doi.org/10.1103/PhysRevB.79.014108

29. M.A. Lebyodkin, N.P. Kobelev, Y. Bougherira, D. Entemeyer, C. Fressengeas, V.S. Gornakov, T.A. Lebedkina, and I.V. Shashkov, *Acta Mater.*, **60**, No. 9: 3729 (2012); https://doi.org/10.1016/j.actamat.2012.03.026
30. V.E. Vildeman, E.V. Lomakin, T.V. Tret'yakova, and M.P. Tret'yakov, *Mech. Solids*, **51**: 612 (2016); https://doi.org/10.3103/S0025654416050150
31. E. Rizzi and P. Hähner, *Int. J. Plast.*, **20**, No. 1: 121 (2004); https://doi.org/10.1016/S0749-6419(03)00035-4
32. H. Kolsky, *Stress Waves in Solids* (New York: Dover Publ.: 2003).
33. H. Kolsky and D. Rader, *Fracture. An Advance Treatise* (Ed. H. Liebowitz) (New York: Academic Press: 1968).
34. V.A. Vasiliev, Y.M. Romanovsky, and V.G. Yakhno, *Sov. Phys.–Usp.*, **22**, No. 8: 615 (1979); https://doi.org/10.1070/PU1979v022n08ABEH005591
35. P. Hähner, *Appl. Phys.* A, **58**: 41 (1994); https://doi.org/10.1007/BF00331515
36. L.B. Zuev, V.I. Danilov and N.V. Kartashova, *JETP Lett.*, **60**: 553 (1994).
37. F.S. Crawford, *Waves* (New York: McGraw-Hill Comp.: 1968).
38. L.B. Zuev, *Annalen der Physik*, **10**, Nos. 11–12: 965 (2001); https://doi.org/10.1002/1521-3889(200111)10:11/12<965::AID-ANDP965>3.0.CO;2-N
39. L.B. Zuev, *Annalen der Physik*, **16**, No. 4: 286 (2007); https://doi.org/10.1002/andp.200610233
40. L.B. Zuev, V.I. Danilov, and S.A. Barannikova, *Int. J. Plast.*, **17**, No. 1: 47 (2001); https://doi.org/10.1016/S0749-6419(00)00018-8
41. L.B. Zuev, *Phys. Wave Phenom.*, **20**: 166 (2012); https://doi.org/10.3103/S1541308X12030028
42. G.A. Malygin, *Phys. Sol. Stat.*, **43**: 1909 (2001); https://doi.org/10.1134/1.1410630
43. H.G. Othmer, *Nonlinear Wave Processes in Excitable Media* (Eds. A.V. Holden, M. Marcus, and H.G. Othmer) (New York: Plenum Press: 1991), p. 213.
44. V.A. Davydov, N.V. Davydov, G.V. Morozov, M.N. Stolyarov, and T. Yamaguchi, *Cond. Matter Phys.*, **7**, No. 3 (39) 565 (2004); https://doi.org/10.5488/CMP.7.3.565
45. B.B. Kadomtsev, *Phys.–Usp.*, **37**, No. 5: 425 (1994); https://doi.org/10.1070/PU1994v037n05ABEH000109
46. L.B. Zuev, *Bull. Russ. Acad. Sci. Phys.*, **78**: 957 (2014); https://doi.org/10.3103/S1062873814100256
47. D.J. Hudson, *Statistics* (Geneva: CERN: 1964).
48. S.A. Barannikova, *Tech. Phys. Lett.*, **30**: 338 (2004); https://doi.org/10.1134/1.1748618
49. L.B. Zuev, S.F. Barannikova, V.I. Danilov and V.V. Gorbatenko, *Phys. Wave Phenom.*, **17**: 66 (2009); https://doi.org/10.3103/S1541308X09010117
50. V.V. Pustovalov, *Low. Temp. Phys.*, **34**, No. 9: 683 (2008); https://doi.org/10.1063/1.2973710
51. L.B. Zuev, B.S. Semukhin, and N.V. Zarikovskaya, *Int. J. Sol. Struct.*, **40**, No. 4: 941 (2003); https://doi.org/10.1016/S0020-7683(02)00612-1

52. G.B. Whithem, *Linear and Nonlinear Waves* (New York: John Wiley and Sons: 1974).
53. M. Eigen and P. Schuster, *The Hypercycle* (Berlin*: Springer-Verlag*: 1979).
54. D.D. Vvedensky, *Partial Differential Equations* (Wokingham: Addison-Wesley: 1993).
55. R. Hill, *The Mathematical Theory of Plasticity* (Oxford: University Press: 1998).
56. W. Oliferuk and M. Maj, *Europ. J. Mech. A. Solids*, **28**, No. 2: 266 (2009); https://doi.org/10.1016/j.euromechsol.2008.06.003
57. A.A. Shibkov and A.E. Zolotov, *JETP Lett.*, **90**: 370 (2009); https://doi.org/10.1134/S0021364009170123
58. F. McClintock and A.S. Argon, *Mechanical Behavior of Materials* (Sydney: Addison-Wesley: 1966).
59. A.Z. Patashinskii and V.L. Pokrovskii, *Fluctuation Theory of Phase Transitions* (London: Pergamon Press: 1979).
60. L.B. Zuev and B.S. Semukhin, *Phil. Mag.* A, **82**, No. 6: 1183 (2002); https://doi.org/10.1080/01418610208240024
61. L.I. Sedov, *Mechanics of Continuous Media* (Singapore: World Scientific: 1997).
62. L.D. Landau and E.M. Lifshitz, *Fluid Mechanics* (Oxford: Elsevier: 1987); https://doi.org/10.1016/C2013-0-03799-1
63. V.I. Alshits and V.L. Indenbom, *Dislocations in Crystals* (Ed. F.R.N. Nabarro) (Amsterdam: North-Holland: 1986), p. 43.
64. D. Caillard and J.L. Martin, *Thermally Activated Mechanisms in Crystal Plasticity* (Oxford: Elsevier: 2003).
65. H. Donth, *Z. Phys.*, **149**: 111 (1957).
66. O.M. Braun and Y. Kivshar, *The Frenkel–Kontorova Model: Concepts, Methods, and Applications* (Berlin: Springer-Verlag: 2004); https://doi.org/10.1007/978-3-662-10331-9
67. S.K. Khannanov, *Fiz. Met. Met.*, No. 4: 14 (1992).
68. S.K. Khannanov and S.P. Nikanorov, *Tech. Phys.*, **52**: 70 (2007); https://doi.org/10.1134/S1063784207010124
69. G.F. Sarafanov and V.N. Perevezentsev, *Tech. Phys. Lett.*, **31**: 936 (2005); https://doi.org/10.1134/1.2136958
70. I.L. Maksimov, G.F. Sarafanov, and S.N. Nagornykh, *Solid State Phys.*, **37**: 3169 (1995).
71. G.F. Sarafanov, *Phys. Sol. Stat.*, **43**: 263 (2001).
72. G.F. Sarafanov, *Phys. Sol. Stat.*, **50**: 1868 (2008); https://doi.org/10.1134/S1063783408100144
73. G.A. Malygin, *Phys.–Usp.*, 42, No. 9: **887** (1999); https://doi.org/10.1070/pu1999v042n09ABEH000563
74. G.A. Malygin, *Phys. Sol. Stat.*, **47**: 246 (2005); https://doi.org/10.1134/1.1866402
75. G.A. Malygin, *Phys. Sol. Stat.*, **47**: 896 (2005); https://doi.org/10.1134/1.1924852
76. G.A. Malygin, *Phys. Sol. Stat.*, **48**: 693 (2006); https://doi.org/10.1134/S1063783406040123
77. Y.A. Khon, Y.R. Kolobov, M.B. Ivanov and A.V. Butenko, *Tech. Phys.*, **53**: 328 (2008); https://doi.org/10.1134/S1063784208030079
78. L.B. Zuev, Y.A. Khon, and S.A. Barannikova, *Tech. Phys.*, **55**: 965 (2010); https://doi.org/10.1134/S106378421007008X

79. E. Zasimchuk, Yu. Gordienko, L. Markashova, and T. Turchak, *J. Mat. Engng. Perf.*, **18**: 947 (2009); https://doi.org/10.1007/s11665-008-9327-0
80. E. Zasimchuk, O. Baskova, O. Gatsenko, and T. Turchak, *J. Mat. Eng. Perf.*, **27**: 4183 (2018); https://doi.org/10.1007/s11665-018-3515-3
81. A.I. Olemskoi, *Theory of Structure Transformation in Non-Equilibrium Condensed Matter* (New York: NOVA Science: 1999).
82. A.I. Olemskoi and I.A. Sklyar, *Phys.–Usp.*, **35**, No. 6: 455 (1992); https://doi.org/10.1070/PU1992v035n06ABEH002241
83. A.I. Olemskoi, *Phys.–Usp.*, **44**, No. 5: 479 (2001); https://doi.org/10.1070/PU2001v044n05ABEH000921
84. G.P. Cherepanov, A.S. Balankin, and V.S. Ivanova, *Eng. Fract. Mech.*, **51**: 997 (1995).
85. A.S. Balankin, *Tech. Phys. Lett.*, **15**: 15 (1989).
86. Y. Bayandin, V. Leont'ev, O. Naimark, and S. Permjakov, *J. Phys. IV France*, **134**, 1015 (2006); https://doi.org/10.1051/JP4:2006134155
87. O.A. Plekhov, N. Saintier, and O. Naimark, *Tech. Phys.*, **52**: 1236 (2007); https://doi.org/10.1134/S106378420709023X
88. O.A. Plekhov, *Tech. Phys.*, **56**: 301 (2011). https://doi.org/10.1134/S106378421102023X
89. O. Naimark and M. Davydova, *J. Phys. IV France*, **6**: 259 (1996); https://doi.org/10.1051/JP4:1996625
90. O.B. Naimark, *Advances in Multifield Theories of Continua with Substructure* (Eds. G. Capriz and P. Mariano) (Boston: Birkhauser Inc.: 2003), p. 75.
91. I.A. Panteleev, O.A. Plekhov, and O.B. Naimark, *Izv., Phys. Sol. Earth*, **48**: 504 (2012); https://doi.org/10.1134/S1069351312060055
92. E.V. Kozlov, V.A. Starenchenko, and N.A. Koneva, *Metals*, No. 5: 152 (1993).
93. B. Lüthi, *Physical Acoustics in the Solids* (Berlin: Springer-Verlag, 2007).
94. G.A. Malygin, *Phys. Sol. Stat.*, **42**: 72 (2000); https://doi.org/10.1134/1.1131170
95. G.A. Malygin, *Phys. Sol. Stat.*, **42**: 706 (2000); https://doi.org/10.1134/1.1131276
96. J.K. Burnett, *Theory and Uses of Acoustic Emission* (New York: Nova Sci. Publ.: 2012).
97. T. Tokuoka and Y. Iwashimizu, *Int. J. Sol. Struct.*, **4**: 383 (1968).
98. I. Kovács, O.Q. Chinh, and E. Kovács-Csetenyi, *Phys. Stat. Sol. A*, **19**: 3 (2002); https://doi.org/10.1002/1521-396X(200211)194:1<3::AID-PSSA3>3.0.CO;2-K.
99. L.I. Mirkin, *Handbook of X-Ray Structural Analysis of Polycrystals* (New York: Consultants Bureau: 1964).
100. O.L. Anderson, *Physical Acoustics: Principles and Methods* (Eds. W.P. Mason and R.N. Thurston) (New York: Academic Press: 1965), p. 43.
101. T. Suzuki, S. Takeuchi, and H. Yoshinaga, *Dislocation Dynamics and Plasticity* (Berlin: Springer-Verlag: 1991).
102. L. Zhang, N. Sekido, and T. Ohmura, *Mater. Sci. Eng. A*, **611**: 188 (2014); https://doi.org/10.1016/j.msea.2014.05.073
103. R.E. Newnham, *Properties of Materials* (Oxford: University Press: 2005).

104. L.B. Zuev, *Tech. Phys. Lett.*, **31**: 89 (2005); https://doi.org/10.1134/1.1877610
105. M.S. Ryvkin and Y.B. Rumer, *Thermodynamics, Statistical Physics and Kinetics* (Moscow: MIR Publ.: 1980).
106. P. Landau, R.Z. Shneck, G. Makov, and A. Venkert, *IOP Conf. Ser.*, **3**: 012004 (2009); https://doi.org/10.1088/1757-899X/3/1/012004
107. L.D. Landau and E.M. Lifshitz, *Statistical Physics* (Oxford: Pergamon Press: 1969).
108. E. Hug and C. Keller, *Phil Mag. A*, **99**, No. 11: 1297 (2019); https://doi.org/10.1080/14786435.2019.1580397
109. L.B. Zuev and V.I. Danilov, *Int. J. Sol. Struct.*, **34**, No. 29: 3795 (1997); https://doi.org/10.1016/S0020-7683(97)00003-6
110. L.B. Zuev and V.I. Danilov, *Phil. Mag. A*, **79**, No. 1: 43 (1999); https://doi.org/10.1080/01418619908214273
111. A. Ishii, J. Li, and S. Ogata, *Int. J. Plast.*, **82**: 32 (2016); https://doi.org/10.1016/j.ijplas.2016.01.019
112. R.A. Andrievski and A.M. Glezer, *Phys.–Usp.*, **52**, No. 4: 315 (2009); https://doi.org/10.3367/UFNe.0179.200904a.0337
113. L.B. Zuev, S.A. Barannikova, and A.G. Lunev, *Prog. Phys. Met.*, **19**, No. 4: 379 (2018) (in Russian); https://doi.org/10.15407/ufm.19.04.379
114. V.E. Nazarov, *Phys. Sol. Stat.*, **58**: 1719 (2016); https://doi.org/10.1134/S1063783416090249
115. J.J. Gilman, *J. Appl. Phys.*, **36**, No. 9: 2772 (1965); https://doi.org/10.1063/1.1714577
116. P.W. Atkins, *Quanta* (Oxford: Clarendon Press: 1974).
117. J.M. Ziman, *Electrons and Phonons* (Oxford: University Press: 2001).
118. J.P. Billingsley, *Int. J. Solids Struct.*, **38**, Nos. 24–25: 4221 (2001); https://doi.org/10.1016/S0020-7683(00)00286-9
119. L.B. Zuev, *Int. J. Solids Struct.*, **42**, Nos. 3–4: 943 (2005); https://doi.org/10.1016/j.ijsolstr.2004.08.009
120. L.B. Zuev and S.A. Barannikova, *Tech. Phys.*, **65**: 741 (2020); https://doi.org/10.1134/S1063784220050266
121. L.B. Zuev and S.A. Barannikova, *Cryst.*, **9**: 458 (2019); https://doi.org/10.3390/cryst9090458
122. H. Umezava, H. Matsumoto, and M. Tackiki, *Thermo Field Dynamics and Condensed States* (Amsterdam: North-Holland Publ. Comp.: 1982).
123. E.M. Morozov, L.S. Polack, and Y.B. Fridman, *Soviet Physics–Doklady*, **156**: 537 (1964).
124. B. Steverding, *Mater. Sci. Eng.*, **9**: 185 (1972).
125. S.N. Zhurkov, *Phys. Sol. Stat.*, **25**: 1997 (1983).
126. J.J. Gilman, *J. Appl. Phys.*, **39**, No. 13: 6086 (1968); https://doi.org/10.1063/1.1656120
127. T. Oku and J.M. Galligan, *Phys. Rev. Lett.*, **22**, No. 12: 596 (1969); https://doi.org/10.1103/PhysRevLett.22.596
128. B.V. Petukhov and V.L. Pokrovskii, *JETP*, **63**: 634 (1972).
129. E. Nelson, *Dynamical Theories of Brownian Motion* (Princeton University Press: 1967).
130. P.A.M. Dirac, *Directions in Physics* (New York: John Wiley and Sons: 1978).
131. Y. Imry, *Introduction to Mesoscopic Physics* (Oxford: University Press: 2002).

132. E. Scerri, *The Periodic Table: Its Story and Its Significance* (Oxford: University Press: 2007).
133. A.P. Cracknell and K.G. Wong, *The Fermi Surface* (Oxford: Clarendon Press: 1973).
134. W. Hume-Rothery, *Elements of Structural Metallurgy* (London: Inst. Metals: 1961).
135. L.D. Landau and E.M. Lifshitz, *Quantum Mechanics. Non-Relativistic Theory* (Elsevier: 1977);
https://doi.org/10.1016/C2013-0-02793-4
136. G. Grimwall, B. Magyari-Köpe, V. Ozoliņŝ, and K.A. Persson, *Rev. Mod. Phys.*, **84**, No. 2: 945 (2012);
https://doi.org/10.1103/RevModPhys.84.945
137. H. Conrad, *Mater. Sci. Eng. A*, **287**, No. 2: 276 (2000);
https://doi.org/10.1016/S0921-5093(00)00786-3
138. M.-J. Kim, K. Lee, K.H. Oh, I.-S. Choi, H.-H. Yu, S.-T. Hong, and H.N. Han, *Scr. Mater.*, **75**: 58 (2014);
https://doi.org/10.1016/j.scriptamat.2013.11.019
139. L.B. Zuev and S.A. Barannikova, *Tech. Phys. Lett.*, **45**: 721 (2019);
https://doi.org/10.1134/S1063785019070319
140. A.A. Shibkov, M.F. Gassanov, A.A. Denisov, A.E. Zolotov and B.I. Ivolgin, *Tech. Phys.*, **62**: 652 (2017);
https://doi.org/10.1134/S1063784217040260

Received 10.11.2020;
in final version, 10.02.2021

Л.Б. Зуєв, С.А. Бараннікова, В.І. Данілов, В.В. Горбатенко
Інститут фізики міцности та матеріалознавства СВ РАН,
Академічний просп., 2/4; 634055 Томськ, Російська Федерація

ПЛАСТИЧНІСТЬ: ВІД КРИСТАЛІЧНОЇ ҐРАТНИЦІ ДО МАКРОСКОПІЧНИХ ЯВИЩ

Обговорено нові уявлення у фізиці пластичности кристалів. Запропоновано модель пластичної плинности, яка може описувати її основні закономірності. За допомогою експериментального дослідження показано, що локалізація пластичної плинности відіграє роль у розвиненні пластичної деформації. Одержані дані пояснено за допомогою принципів теорії нерівноважних систем. Вводиться квазичастинка для описування явища пластичности. Встановлено зв'язок між характеристиками локалізованої пластичности металів та їхнім положенням у Періодичній таблиці елементів. Розроблено новий модель для описування локалізованої еволюції пластичної плинности у твердих тілах. Згідно із запропонованим моделем елементарні акти пластичности, що розвиваються у деформованому середовищі, ґенерують імпульси акустичної емісії, які взаємодіють із носіями пластичности й ініціюють нові елементарні зсуви. Експериментально встановлено, що макролокалізація пластичної плинности проявляється у вигляді різних мод автохвильових процесів. Задля пояснення феномена автохвиль локалізації пластичної плинности введено нову квазичастинку — «автолокалізон»; модель уможливлює оцінити просторові та часові параметри деформаційного процесу.

Ключові слова: стопи, деформація, плазучість, самоорганізація, міцність, пластичність, локалізація, руйнування.